

การวิเคราะห์สมบัติเชิงโครงสร้างของแกเลียมไนไตรด์ที่ปลูกลงบนแกเลียมอาร์เซไนด์ โดยวิธี
เอ็มโอวีพีอี ด้วยกล้องจุลทรรศน์อิเล็กตรอนชนิดส่งผ่าน



นางสาวศิริเพ็ญ สวนดอน

สถาบันวิทยบริการ

วิทยานิพนธ์นี้เป็นส่วนหนึ่งของการศึกษาตามหลักสูตรปริญญาวิทยาศาสตรมหาบัณฑิต

สาขาวิชาฟิสิกส์ ภาควิชาฟิสิกส์

คณะวิทยาศาสตร์ จุฬาลงกรณ์มหาวิทยาลัย

ปีการศึกษา 2548

ISBN 974-17-4382-3

ลิขสิทธิ์ของจุฬาลงกรณ์มหาวิทยาลัย

STRUCTURAL PROPERTY ANALYSIS OF GaN GROWN ON GaAs BY
MOVPE USING TRANSMISSION ELECTRON MICROSCOPY



Miss Siripen Suandon


สถาบันวิทยบริการ
จุฬาลงกรณ์มหาวิทยาลัย

A Thesis Submitted in Partial Fulfillment of the Requirements
for the Degree of Master of Science Program in Physics

Department of Physics
Faculty of Science
Chulalongkorn University
Academic year 2005
ISBN 974-17-4382-3

Thesis Title STRUCTURAL PROPERTY ANALYSIS OF GaN GROWN
ON GaAs BY MOVPE USING TRANSMISSION ELEC-
TRON MICROSCOPY
By Miss. Siripen Suandon
Field of Study Physics
Thesis Advisor Sakuntam Sanorpim, Ph.D.
Thesis Co-advisor Assistant Professor Kajornyod Yoodee, Ph.D.

Accepted by the Faculty of Science, Chulalongkorn University in Partial
Fulfillment of the Requirements for the Master's Degree



..... Dean of the Faculty of Science
(Professor Piamsak Menasveta, Ph.D.)

THESIS COMMITTEE

Wichit Sritrakool Chairman
(Associate Professor Wichit Sritrakool, Ph.D.)

Stm. Thesis Advisor
(Sakuntam Sanorpim, Ph.D.)

Kajornyod Yoodee Co-advisor
(Assistant Professor Kajornyod Yoodee, Ph.D.)

Thiti B. Member
(Thiti Bovornratanaraks, Ph.D.)

Orapin Wannadelok Member
(Orapin Wannadelok, Ph.D.)

ศิริเพ็ญ สนวนดอน : การวิเคราะห์สมบัติเชิงโครงสร้างของแกเลียมไนไตรด์ที่ปลูกลงบน
แกเลียมอาร์เซไนด์ โดยวิธีเอ็มโอฟีอี ด้วยกล้องจุลทรรศน์อิเล็กตรอนชนิดส่งผ่าน
(STRUCTURAL PROPERTY ANALYSIS OF GaN GROWN ON GaAs BY MOVPE
USING TRANSMISSION ELECTRON MICROSCOPY)

อาจารย์ที่ปรึกษา: ดร. สกฤธรรม เสนาะพิมพ์ อาจารย์ที่ปรึกษาร่วม: ผศ.ดร. ขจรยศ อยู่ดี
,57 หน้า. ISBN 974-17-4382-3

ผู้วิจัยใช้กล้องจุลทรรศน์อิเล็กตรอนชนิดส่งผ่าน (TEM) ตรวจสอบและวิเคราะห์สมบัติเชิง
โครงสร้างในระดับไมโคร/นาโนของฟิล์มบางแกเลียมไนไตรด์ (GaN) ที่ปลูกผลึกลงบนแกเลียม
อาร์เซไนด์ (GaAs) ชั้นสเตรตที่มีผิวระนาบ (001) โดยวิธีเมทอลอจแกเลนิคเวปเปอร์เฟสเอพิแทกซี
(MOVPE) ผลการศึกษาการเลี้ยวเบนของรังสีเอ็กซ์ (XRD) และผลจากการเลี้ยวเบนของ
อิเล็กตรอน (ED) บ่งชี้ว่า ฟิล์มบาง GaN ที่เตรียมได้มีโครงสร้างแบบซิทท์เบลนด์หรือเรียกว่า โครง
สร้างผลึกแบบคิวบิก (cubic structure GaN, c-GaN) นอกจากนี้ภาพไมโครกราฟชนิดภาคตัด
ขวางและผลจาก ED ของ TEM แสดงให้เห็นว่า ฟิล์มบาง GaN ที่ปลูกผลึกในช่วงอุณหภูมิต่ำ
(900-920 องศาเซลเซียส) มีแถบของความบกพร่องชนิดสแตกกิงฟอลท์และทวิน ซึ่งวางตัวอยู่บน
ระนาบ (111) โดยที่ความหนาแน่นของสแตกกิงฟอลท์และทวินมีปริมาณลดลงที่บริเวณที่ห่างจาก
ผิวรอยต่อระหว่าง GaN และ GaAs จากการวิเคราะห์โครงสร้างผลึกไม่พบการก่อเกิดของโครง
สร้างผลึกแบบเฮกซะโกนัล ในฟิล์มบางที่ถูกปลูกผลึกที่อุณหภูมิต่ำ ในทางตรงกันข้ามผลการ
แทรกสอดของคลื่นเลี้ยวเบนจากบริเวณที่เลือก (SAD) ของ TEM, XRD และ โพโตลูมิเนสเซนซ์ พบ
ว่า ฟิล์มบาง GaN ที่ถูกเตรียมภายใต้สภาวะที่อุณหภูมิในการปลูกผลึกสูงขึ้นประมาณ 960 องศา
เซลเซียส แสดงการเปลี่ยนโครงสร้างเดี่ยวแบบคิวบิกไปเป็นโครงสร้างผสมระหว่างคิวบิกและเฮก
ซะโกนัล (*h*-GaN) นอกจากนี้ยังตรวจพบว่าคุณลักษณะการเรืองแสงของฟิล์มบาง GaN ไวต่อการ
เกิดโครงสร้างเดี่ยวของ *h*-GaN งานวิจัยนี้ได้แสดงให้เห็นว่าอุณหภูมิในการปลูกผลึกและการก่อ
เกิดของระนาบ (111) บนผิวหน้าของชั้น c-GaN และที่ผิวรอยต่อระหว่างชั้น c-GaN และ GaAs
ชั้นสเตรต มีบทบาทสำคัญในการปลูกผลึกฟิล์มบาง c-GaN ให้มีความบริสุทธิ์สูงปราศจากความ
บกพร่องเชิงระนาบและการก่อเกิดของโครงสร้างเดี่ยวของ *h*-GaN ในฟิล์มบาง c-GaN

ภาควิชา.....ฟิสิกส์.....
สาขาวิชา.....ฟิสิกส์.....
ปีการศึกษา.....2548.....

ลายมือชื่อนิสิต.....ศิริเพ็ญ สนวนดอน.....
ลายมือชื่ออาจารย์ที่ปรึกษา.....Stm.....
ลายมือชื่ออาจารย์ที่ปรึกษาร่วม.....นายนว ๐๐๕.....

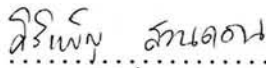
4672429123 :MAJOR PHYSICS

KEY WORDS: TRANSMISSION ELECTRON MICROSCOPY / CUBIC GaN / METAL ORGANIC VAPOR PHASE EPITAXY / STRUCTURAL PROPERTY


SIRIPEN SUANDON : STRUCTURAL PROPERTY ANALYSIS OF GaN GROWN ON GaAs BY MOVPE USING TRANSMISSION ELECTRON MICROSCOPY. THESIS ADVISOR : SAKUNTAM SANORPIM, PH.D. THESIS CO-ADVISOR : ASST. PROF. KAJORN YOD YOODEE, PH.D., 57 pp. ISBN 974-17-4382-3.

Transmission electron microscopy (TEM) observation has been performed on the micro-(nano-) structure of GaN films grown on GaAs (001) substrates by metalorganic vapor phase epitaxy (MOVPE). Based on our results of x-ray diffraction (XRD) and electron diffraction (ED), the GaN grown films have a zincblende structure, i.e., a cubic structure or *c*-GaN. For lower growth temperatures (900-920°C), cross-sectional TEM micrographs and ED patterns demonstrate that the GaN grown films contain bands of stacking faults (SFs) and twins parallel to (111) planes. Besides, the density of SF and twin defects decreases with the distance from the interface of *c*-GaN/GaAs. No different type of single diffraction spots on the ED pattern was observed. On the other hand, the GaN films exhibited a transition from cubic to mixed cubic/hexagonal phase under conditions of increasing growth temperature ($T_g \simeq 960^\circ\text{C}$) as determined by using TEM-selected area diffraction (SAD) technique with complementary XRD and PL observations. In addition, the luminescence characteristics of *c*-GaN films are shown to be very sensitive to the presence of the single-crystal hexagonal GaN (*h*-GaN). T_g and the formation of (111) facets on the top surface of *c*-GaN and on the interface of *c*-GaN/GaAs play an important role in growing high cubic-phase purity *c*-GaN films with low density of planar defects (SFs and twins) and without incorporation of single-crystal *h*-GaN.


Department.....Physics....

Student's signature 

Field of study....Physics....

Advisor's signature 

Academic year...2005.....

Co-advisor's signature 

Acknowledgements

I would like to sincerely express my gratitude to my advisor, Dr.Sakuntam Sanorpim and Assistant Professor Dr.Kajornyod Yoodee for their valuable suggestion and encouragement. They gave me good experiences, such as working with good guidance, participating in an international conference (presentation) in Singapore, and English writing (journal and thesis).

I would like to thank the Condensed Matter Research Group (CMRG) for the facilities. Especially, I would like to pay respective thank to Dr.Sojiphong Chatraphorn who provided the convenient office for making this thesis.

I would like to thank Associate Professor Dr.Wichit Sritrakool, Dr.Thiti Bovornratanaraks, and Dr.Orapin Wannadelok for taking times from their busy schedules to be on my thesis committee. Their comments on this thesis are also greatly appreciated. I wish to thank Assistant Professor Dr. Sukkaneste Tungasmita and Assistant Professor Dr.Patcha Chatraphorn for useful suggestion and additional information to support my work.

I would like to acknowledge the financial supports from the Thailand-Japan Technology Transfer Project-Overseas Economic Cooperation Fund (TJTTP-OECF) and Graduate Schools of Chulalongkorn University for paying fund for this thesis. I would like to acknowledge Department of Physics, Faculty of Science, Chulalongkorn University for providing teaching assistantship. Special thank goes to Dr.Kentaro Onabe, Department of Advanced Materials Science, Graduate Schools of Frontier Sciences, The University of Tokyo, Japan for providing the great sample to analyze and correcting my manuscripts.

I would like to thank my gang, Ying, Ann, Am, Nui, Tew, Dares Kwang, Tai, Am, Art, Kai, Kae, Nong, Gade, Toy, Kan, Bee, Pu, Mod and many friends for useful discussions and joyful moment. Especially, I also thank Pat, Pun, Chin, Ud and Sun for helps and suggestion to use Latex for writing this thesis.

Last but not least, I would like to pay my heartfelt thanks to my family ; my father, mother, my sister and Nong-Earn for love, understanding and supports.

Table of Contents

Abstract (Thai)	iv
Abstract (English)	v
Acknowledgements	vi
Table of Contents	vii
List of Tables	ix
List of Figures	x
 Chapter	
I Introduction	1
1.1 Overviews of GaN	1
1.2 Objectives and organization of the thesis	5
II Transmission electron microscopy (TEM)	7
2.1 Introduction	7
2.2 System and principle of TEM	8
2.3 Preparation of semiconducting sample for TEM	9
2.3.1 Cross-sectional preparation	10
2.3.2 Plan-view preparation	13
2.4 Analytical theory of TEM	14
2.4.1 Image mode	15
2.4.2 Diffraction mode	15

III Structural defects in <i>c</i>-GaN film	26
3.1 Initial investigated results of <i>c</i> -GaN film	26
3.1.1 Surface morphology of <i>c</i> -GaN film	27
3.1.2 Crystal structure of <i>c</i> -GaN grown film	28
3.2 TEM investigations of <i>c</i> -GaN film	29
3.3 Summary	33
IV Generation of <i>h</i>-GaN in <i>c</i>-GaN	34
4.1 Initial investigated results of <i>c</i> -GaN films	34
4.1.1 Effect of growth temperature on crystal structure	35
4.1.2 Correlation between luminescence properties and crystal structure	36
4.2 TEM investigations of <i>c</i> -GaN films	38
4.3 Summary	41
V Structural phase transtitions in SAG-<i>c</i>-GaN films	42
5.1 Overview of SAG- <i>c</i> -GaN	42
5.2 Growth feature of SAG <i>c</i> -GaN	44
5.3 TEM investigation of SAG <i>c</i> -GaN	45
5.4 Summary	49
VI Conclusion	50
References	53
Vitae	57

List of Tables

- 1.1 Lattice constants, lattice mismatch and thermal expansion coefficients
for substrate materials of *c*-GaN film 4

- 2.1 Complete the ratio of space tables of some plane for fcc 25



สถาบันวิทยบริการ
จุฬาลงกรณ์มหาวิทยาลัย

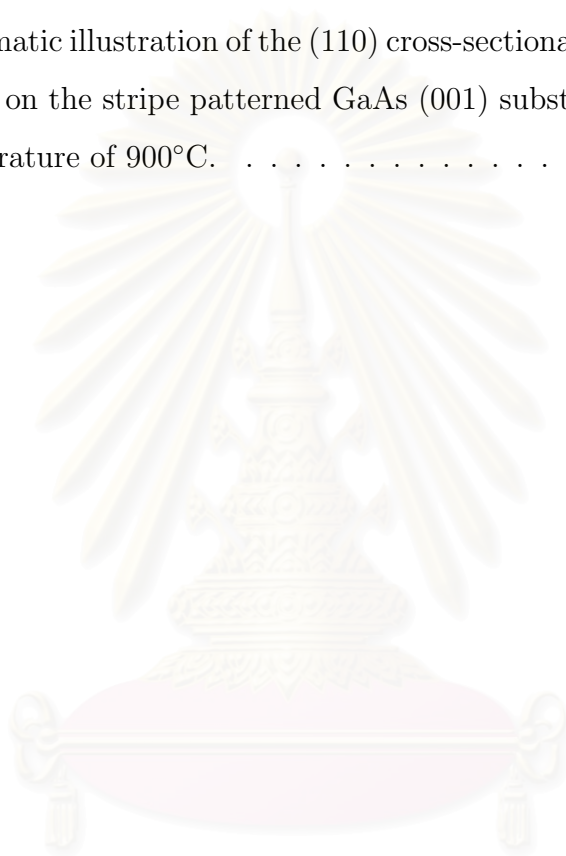
List of Figures

1.1	Schematic illustration of GaN structural property	2
1.2	Schematic view of structure of planar defects in <i>c</i> -GaN along (110) cross-section	3
2.1	Schematic illustration of electron signal in a TEM system [24]	8
2.2	a) Cutting instrument low speed diamond wheel saw. b) Cut sample on the microscope glass.	11
2.3	a) Schematic diagram of sticking 2 surface samples. b) Clamped sample. c) 80°C heating sample on the hot plate. d) Sample on the triangle holder compared with a coin as in the figure.	12
2.4	a) Diamond films. b) Diamond film on lapping.	13
2.5	Ion beam milling machine.	14
2.6	The Ewald sphere construction in 2 dimensions. Section through the sphere of the reflection containing the incident beam vector (\vec{k}), the diffracted beam vector (\vec{G}) and reciprocal lattice vector (\vec{g}_{240}), corresponding to $-2\vec{b}_1+4\vec{b}_2$ when \vec{b}_1 and \vec{b}_2 are the reciprocal unit vectors [25].	17
2.7	Ewald sphere construction in 3 dimensions and the projection of intersected points on the projecting plane as a diffraction spots. The intersected points are indicated by arrows.	18
2.8	(a) Location of the reciprocal-lattice axis b_3 (b) [hkl] direction in the reciprocal lattice [25].	19
2.9	Schematic illustration of (a) (200), (b) (020), (c) (002) and (d) (111) planes in the fcc unit cell and the corresponding reciprocal lattice points	20

2.10	A sector of the full fcc reciprocal lattice (3-D). The other sectors can be imagined extending in the directions of the dotted lines.	21
2.11	[002] Reciprocal lattice section (2-D) taken from the full reciprocal lattice.	21
2.12	The scattering of an incident electron beam (I) by a crystal lattice. In other side of specimen, two kinds of intense beam can be found: the direct beam (T) and the diffracted beam (D). In other directions (N) no intense electron beam will be detected.	22
2.13	Diffraction pattern of GaN along [110] zone axis.	23
2.14	Schematic illustration of electron diffraction in TEM [28]	24
3.1	Schematic illustration of the GaN layer grown on a GaAs (001) substrate.	26
3.2	SEM cross-sectional micrograph and surface morphology of GaN epitaxial layer on GaAs substrate at growth temperature $\sim 900^{\circ}\text{C}$	28
3.3	X-ray diffraction profiles of GaN film grown at 900°C on GaAs (001) substrate.	29
3.4	TEM results of GaN film and GaAs substrate region at growth temperature $\sim 900^{\circ}\text{C}$ a) Cross-sectional micrograph. b) Electron diffraction (ED) patterns.	30
3.5	Illustrations of possible crystal defects in the <i>c</i> -GaN film at the (110) cross-section a) Stacking fault b) Hexagonal inclusion c) Twin. 31	31
3.6	Illustration of planar defects (stacking fault and twin) in the <i>c</i> -GaN film on GaAs substrate at growth temperature $\sim 900^{\circ}\text{C}$ at the (110) cross-section	32
4.1	Schematic illustration of the GaN layer grown on a GaAs (001) at growth temperature of 960°C	35
4.2	$2\theta/\omega$ -scan XRD (002) profiles of <i>c</i> -GaN films grown at different growth temperatures of 900°C and 960°C	36

4.3	Low-temperature (5.5 K) PL spectra of the corresponding <i>c</i> -GaN films at different growth temperatures of 900°C and 960°C.	37
4.4	Cross-sectional TEM micrographs for the <i>c</i> -GaN layers grown on GaAs(001) substrates at different growth temperatures of a) 900°C and c) 960°C. b) and d) Corresponding selected area diffraction (SAD) patterns taken near the <110> zone axis.	38
4.5	a) Microstructure of the GaN region containing the pyramid-like structure for the GaN layer grown at 960°C. b) Selected area diffraction (SAD) records along <110> <i>c</i> -GaN from the GaN region containing the pyramid-like structure. Schematic representation of Fig. 4.5 b) showing c) and e) hexagonal and d) cubic phase diffraction spots. Diffraction patterns obtained from the grain boundary regions, showing 70.5° rotation of <i>h</i> -GaN crystal around <11-20>. . .	39
4.6	Schematic illustrations of the (110) cross-section view of main crystal-defects generated in the <i>c</i> -GaN films grown on GaAs (001) substrates at growth temperatures a) 900°C and b) 960°C	40
5.1	A schematic of three types of growth feature for SAG <i>c</i> -GaN grown using stripe opening along a) [110], b) [1-10] and c) [100] directions, respectively [33]	43
5.2	Schematic illustration of SAG <i>c</i> -GaN films on stripe patterned GaAs (001) substrate along the [110] orientation at growth temperature of 900°C. W and M indicate the window and SiO ₂ mask regions, respectively.	44
5.3	Cross-sectional SEM micrograph of SAG- <i>c</i> -GaN on stripe patterned GaAs (001) substrates at growth temperature of ~900°C.	45
5.4	Cross-sectional TEM micrograph in the [110]-oriented stripe pattern showing laterally overgrown GaN layer on SiO ₂ mask.	46
5.5	a) Cross-sectional TEM micrograph of GaN on the window (Region 1 in Fig. 5.4) b) Corresponding electron diffraction (ED) patterns taken near the [110] zone axis.	47

- 5.6 a) Cross-sectional TEM micrograph of GaN on the SiO₂ mask (**Region 2** in Fig. 5.4) b) Corresponding electron diffraction (ED) patterns taken near the [110] zone axis. 48
- 5.7 a) Cross-sectional TEM micrographs of top surface region (**Region 3** in Fig. 5.4) b) Corresponding selected area diffraction (SAD) patterns taken near the [110] zone axis. 48
- 5.8 (Schematic illustration of the (110) cross-sectional SAG *c*-GaN layer grown on the stripe patterned GaAs (001) substrate at the growth temperature of 900°C. 49



สถาบันวิทยบริการ
จุฬาลงกรณ์มหาวิทยาลัย

CHAPTER I

INTRODUCTION

1.1 Overviews of GaN

Gallium nitride (GaN) is a promising material for optoelectronic devices because of its unique properties such as its large direct band gap energy, higher thermal conductivity, large free-exciton and optical-phonon energies. GaN and its related alloys, for instance InGaN and AlGaIn, have become the most favorable III-V semiconductor for manufacturing blue-ultraviolet light-emitting diodes (LEDs) and laser diodes (LDs). The successful development of GaN-based blue light LEDs has made the full color LEDs display possible [1, 2, 3, 4]. Generally, GaN has two crystal structures: cubic structure (zincblende structure) and hexagonal structure (wurtzite structure). Figures 1.1 a) and 1.1 b) show schematic illustration of the cubic structure and the hexagonal structure, respectively. The hexagonal phase (*h*-GaN) is stable and commercially available. High quality *h*-GaN films have been grown on various substrates, such as sapphire, SiC and Si. On the other hand, the cubic phase (*c*-GaN) was theoretically predicted that it has many advantages over *h*-GaN [5] because it has higher electron mobility due to weaker phonon scattering and lower electron effective mass. Moreover, *c*-GaN has easier cleavage facets suitable for forming the cavity of the LDs. Therefore, the growth of *c*-GaN films with high quality is very necessary to improve the efficiency of the optoelectronic devices. However, *c*-GaN is metastable [6, 5] and there is no suitable substrate material [4] for the growth of *c*-GaN film. Recently, the *c*-GaN film has been grown on a cubic lattice substrate, such as GaAs [7, 8], Si [9], 3C-SiC [10], and MgO [11]. However, the growth of high quality *c*-GaN is still difficult. It is due to the large

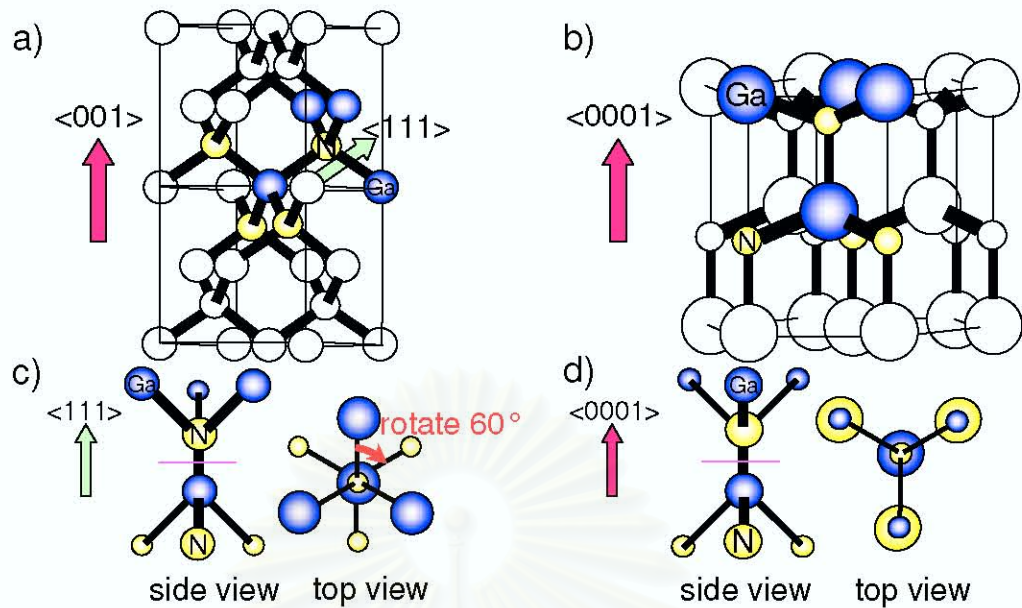


Figure 1.1: Schematic illustration of GaN structural property, a) Cubic structure b) Hexagonal structure c) Rotating cubic structure in $\langle 111 \rangle$ direction d) Hexagonal structure in $\langle 0001 \rangle$ direction.

lattice mismatch and the difference in the thermal expansion coefficients between c -GaN and substrate material. Several research groups reported that there are a few planar defects, such as stacking fault and twin, generated in the c -GaN grown films [12, 13]. The formation of such planar defects is common existing in c -GaN (111) and h -GaN (0001) planes. As shown in Fig.1.1, the c -GaN (111) plane can accommodate the growth of h -GaN structure easily along $\langle 0001 \rangle$ direction. This is because the fundamental difference between these two crystal structures is merely a 60° rotation along the c -GaN (111) and h -GaN (0001) axes [Fig. 1.1 c) and 1.1 d)] [14]. Figure 1.2 shows a model of the structure of planar defects formed by a stacking fault. Due to the structural similarities between the c -GaN (111) and h -GaN (0001) surfaces, they have a number of common physical properties, such as:

(1) They are complementary stacking faults with respect to each other, i.e., the stacking fault in cubic (111) plane is an insertion of 1 monolayer of hexagonal structure and stacking fault in hexagonal (0001) plane is an insertion of 1 monolayer of cubic structure.

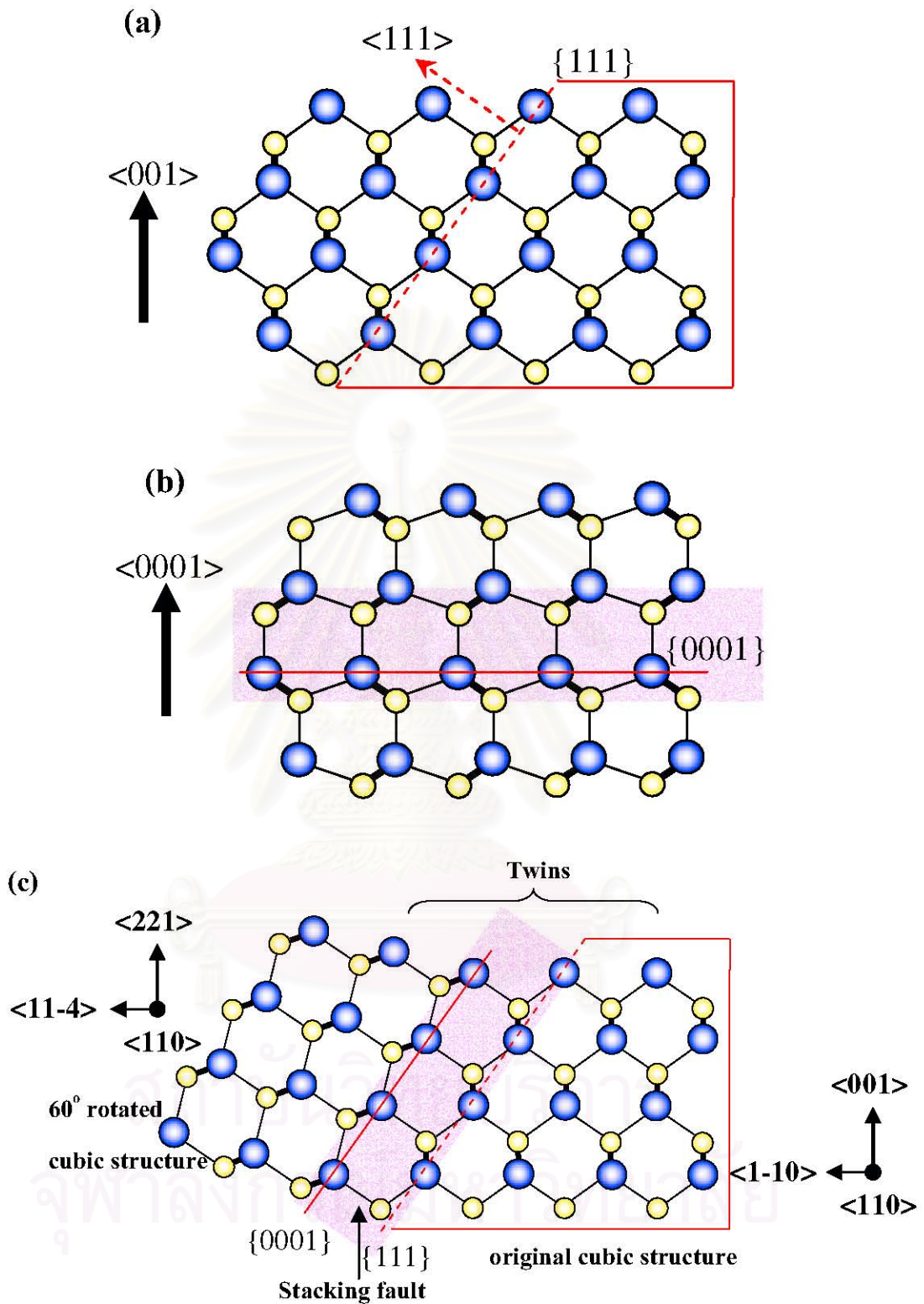


Figure 1.2: Schematic view of structure of planar defects in c -GaN along (110) cross-section, a) Cubic structure, b) Hexagonal structure, c) Stacking fault and twin.

(2) In particular, the twins in *c*-GaN (111) plane are structures of special interest, as they are formed by the insertion of a stacking fault (1 monolayer of hexagonal) between two single crystalline cubic structures rotated by 60° [Fig. 1.2 c)].

However, the inferior crystal quality with the generation of planar defects obstructs explicating the optical properties of *c*-GaN. Therefore, it is believed that the detailed characterization of planar defect formation during the growth of *c*-GaN films is important for further device improvement. To improve the quality of *c*-GaN grown film, there are several research groups that study and seek for the affecting parameters, such as growth method, growth condition, substrate material, surface morphology of substrate, etc. The achievable growth methods, in which the *c*-GaN film was successfully grown, are metalorganic vapor phase epitaxy (MOVPE)[15, 16, 17, 18, 19], molecular beam epitaxy (MBE) [12], plasma-assisted MBE and chemical beam epitaxy (CBE) [20]. However, the MOVPE growth has been traditionally used to deposit the high quality *c*-GaN film. Table

Substrate material	Lattice constant(\AA)	Lattice mismatch (percent)	Thermal expansion coefficient($10^{-6} K^{-1}$)
<i>c</i> -GaN	4.52	0	5.59
3C-SiC	4.3596	3.68	3.9
Si	5.430	16.8	3.59
GaAs	5.652	20.0	6.0
MgO	4.216	7.21	10.5

Table 1.1: Lattice constants, lattice mismatch and thermal expansion coefficients for substrate materials of *c*-GaN film [21].

1.1 summarizes the lattice constants and thermal expansion of *c*-GaN and some substrate materials [21]. As shown in Table 1.1, there is a large difference of lattice constants and thermal expansion coefficients between *c*-GaN and the substrate materials. This results in a density of crystal defects, such as stacking fault, twin and dislocations. In fact, the *c*-GaN film is achievably grown by MOVPE mainly on GaAs substrate despite the large lattice mismatch ($(\Delta a/a) \sim 20$ percent). For

example, Tsuchiya et al. [22] reported the high quality *c*-GaN films were successfully grown on GaAs substrate at the growth temperature about 800°C. However, there is a number of crystal defects, which degrade their optical and structural properties [3]. They concluded that the generation of crystal defects depends on the V/III ratio during growth and the surface morphology of *c*-GaN buffer layer on the GaAs substrate. Although, many affecting parameters were found, in this work we focus on the main parameters, namely the growth temperature and the surface orientation of substrate, which may result in the crystal defects formation during the growth.

1.2 Objectives and organization of the thesis

The major part of this thesis is to describe the micro-(nano-) structure of the MOVPE-grown *c*-GaN films on GaAs (001) substrates, with an emphasis on the formation of the crystal defects, such as stacking faults (SFs) and twins. Also, the polytype conversion of *c*-GaN is discussed. Another aim is to develop an analytical technique of TEM for semiconducting thin films in Thailand. The thesis is organized as follows.

The current knowledge of the transmission electron microscopy (TEM) technique is reviewed in the beginning of Chapter 2,. In addition, preparation of the semiconducting thin film specimen for TEM observation is described in details.

In Chapter 3, the MOVPE growth procedures for high quality *c*-GaN films on GaAs (001) substrates are given. The structural properties of the *c*-GaN film grown at 900°C were quantitatively analyzed by x-ray diffraction (XRD), scanning electron microscopy (SEM) and TEM, focusing particularly on the crystal defects (such as SFs and twins), which were introduced during the growth.

In Chapter 4, the optical and structural properties of *c*-GaN films on GaAs (001) substrate is investigated by photoluminescence, XRD, and TEM. The effect of growth temperature on the polytype conversion of *c*-GaN is discussed. In addition, the crystal defect formations in the films grown at different growth temperatures (900 and 960°C) are compared. The GaN layers exhibited a transition

from cubic to mixed cubic/hexagonal phase under conditions of increasing growth temperature.

Chapter 5 is a continuation of Chapter 4. This chapter focuses on the correlation between the surface orientation of the top surface of *c*-GaN and the extended crystal defects in the GaN films grown on [110]-stripe-patterned GaAs (001) substrates. A selected area diffraction (SAD) analysis in the TEM was used to examine the crystal structure of the selected regions. The results demonstrate that the *h*-GaN is easily constructed along (111) surfaces of the *c*-GaN. The formation of (111) facets on the top surface of *c*-GaN and on the interface of *c*-GaN/GaAs play an important role in growing high cubic-phase purity *c*-GaN films without generation of single-crystal *h*-GaN.

Finally, Chapter 6 gives the conclusions of this thesis.



CHAPTER II

TRANSMISSION ELECTRON MICROSCOPY (TEM)

2.1 Introduction

There are several methods used to study the morphological and structural property of thin film such as x-ray diffraction (XRD) and transmission electron microscopy (TEM), etc. TEM technique has been distinctly demonstrated to be very useful for morphological and micro-(nano-) structural investigations due to its high spatial resolution capability and high magnification of more than 100,000 times depending on an accelerating voltage [23]. However, TEM technique still has a restriction such as complicated operation and difficulty in preparing the sample and interpreting the results. Considerable skill is also required to operate the microscope itself, to take high quality micrographs and to interpret the resultant images. To achieve in this technique, the TEM users have to drastically practice their sample preparation and have to learn about analytical techniques. In this chapter, the system and principle of TEM, preparation of sample, and analytical theory of TEM are described.

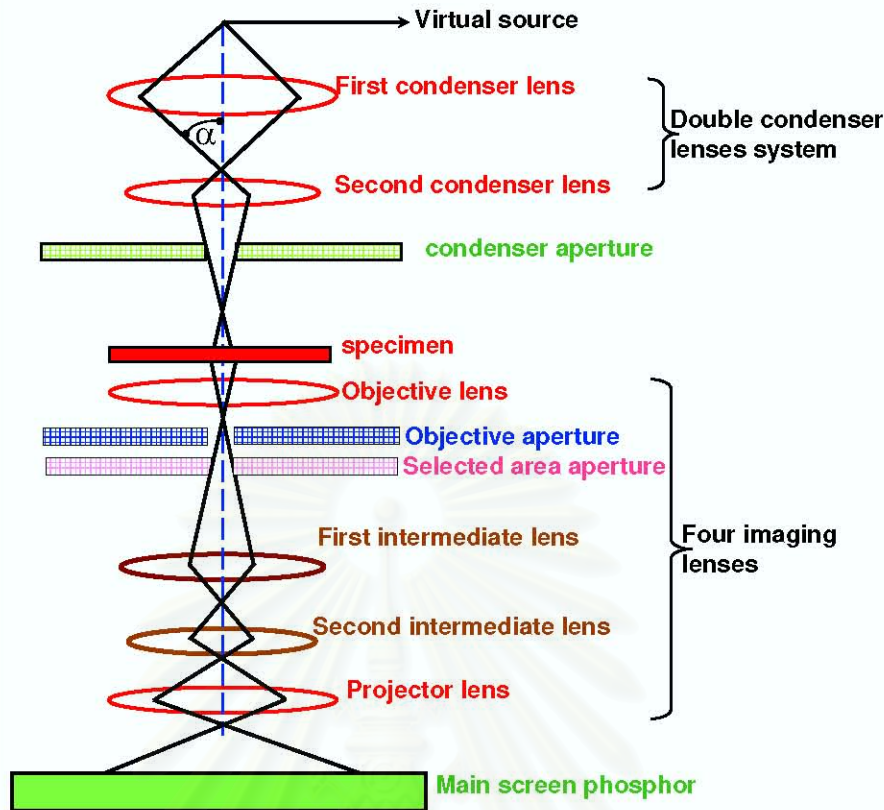


Figure 2.1: Schematic illustration of electron signal in a TEM system [24]

2.2 System and principle of TEM

The concept of resolution and principle in TEM are the same as that in conventional light microscopy. TEM was developed initially because of the limited image resolution in a light microscope, which is imposed by the wavelength of visible light (400-700 nm). Let's see the definition of resolution that is the smallest distance between two points (δ)

$$\delta = \frac{0.61\lambda}{(\eta)\sin\alpha} \quad (2.1)$$

Here, η is the refractive index of the viewing medium that can be approximated to be unity; α is the semi-angle of collection of the magnifying lens, is generally very small; and λ is the wavelength of light. However, an electron wavelength are smaller than an atom, it would be possible to see detail below the atomic scale. In TEM system, the wavelength (λ) of electron beam in *nm* is directly related to

the accelerating voltage, V in kV as following

$$\lambda \simeq \frac{1.22}{\sqrt{V}} \quad (2.2)$$

In light microscopes, the light is focused by the convex light lenses while in the system of TEM, the electron beam is focused by the magnetic lenses. A schematic diagram for a typical TEM system is shown in Fig. 2.1. The TEM system consists of three main components as the following; the first component is a source of illumination which is electron gun (virtual source), the second component is a condenser lenses system which projects the radiation on to the specimen and the third component is a series of imaging lenses which form an image.

A ray diagram for a typical TEM is also shown in Fig. 2.1. Electrons are produced by thermionic emission from a heated tungsten filament in an electron gun. They are accelerated, typically to between 100 and 400 kV , by the electron gun and pass into the column in the anode plate. The electrons are produced by the electron gun, passing through the double condenser lenses system which projects the electrons in a nearly parallel beam onto the specimen. In order to be transparent to the electron beam, the specimen is typically 1000 atoms in thickness. The electron beam transmitting through the specimen is focused by four imaging lenses to form a final magnified image on the main screen phosphor.

สถาบันวิทยบริการ
จุฬาลงกรณ์มหาวิทยาลัย

2.3 Preparation of semiconducting sample for TEM

The processes of preparation of semiconducting material sample, such as epitaxial thin films and bulk films, have to be concerned about the preparation parameters as following; type of abrasive, polishing surface, grid size, lubricant, polishing speed, force and time, which should be suitable for semiconducting materials. To obtain information via TEM, the sample is required to be thin enough for electron transmission. On the other hand, the thickness of about 200 nm must have enough strength because the sample will be bombarded by a highly focused beam of single energy electrons. The essential conditions of the prepared sample for the transmission electron microscope are:

1. The sample must allow sufficient electron transmission to form an image; with minimum energy loss.
2. The sample must be stable under electron bombardment in high vacuum.
3. The sample must have a suitable size to fit the specimen holder (diameter 3 mm) of the microscope.
4. Any preparatory management should not alter the sample structure at a level which is noticeable by the microscope.

In general, the preparation techniques of the sample for TEM have two types: cross-sectional and plan-view techniques. The processes of both techniques are described as the following.

2.3.1 Cross-sectional preparation

A cross-sectional sample for TEM investigation is usually applied to thin films on bulk substrate. This provides an information of the phase distribution in depth and some embedded defect features underneath the loaded surface, which cannot be observed by the plan-view sample. However, the preparation process of the cross-sectional sample is highly dependent on the properties of the film and the

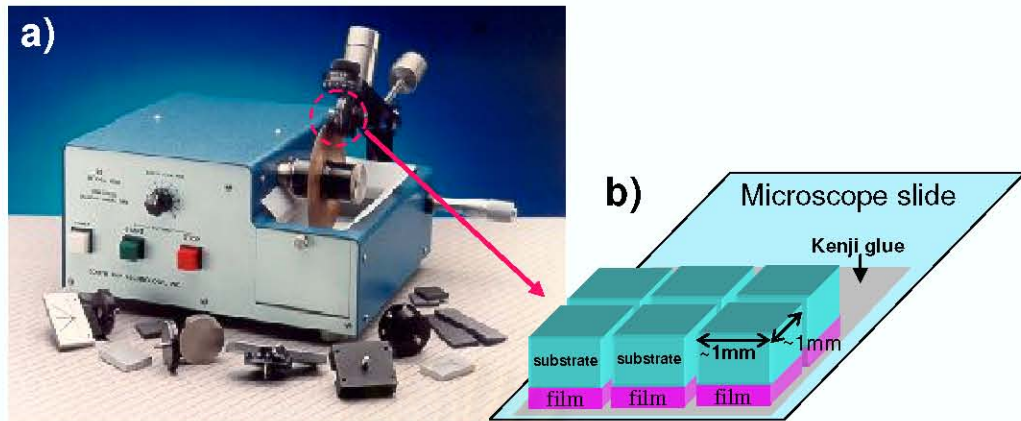


Figure 2.2: a) Cutting instrument low speed diamond wheel saw. b) Cut sample on the microscope glass.

substrate materials. Therefore, a set of test sample preparation must be carried out for determination of the best preparation process.

In this work, TEM was used to investigate the micro-(nano) structural properties of the semiconducting material, namely GaN thin film on GaAs substrate. Owing to a large difference in the hardness of the GaN film and the GaAs substrate, the cross-sectional preparation process must be carefully taken to get the thickness in nano-scale and the smooth-surface sample. The preparation process is divided into four steps which are cutting, clamping, polishing and milling steps.

Cutting process

First of all, to perfectly stick the sample on a microscope slide, the sample surface is wiped by acetone and then followed by methyl alcohol. Next, the sample surface is stuck on the microscope slide with Kenji glue and heated on a hot plate at temperature of 80°C for 30 minutes. Then, the sample is cut to 0.15 mm thickness by diamond-wheel saw, as shown in Fig. 2.2 a), to be $1 \times 1\text{ mm}^2$ (Fig. 2.2 b)).

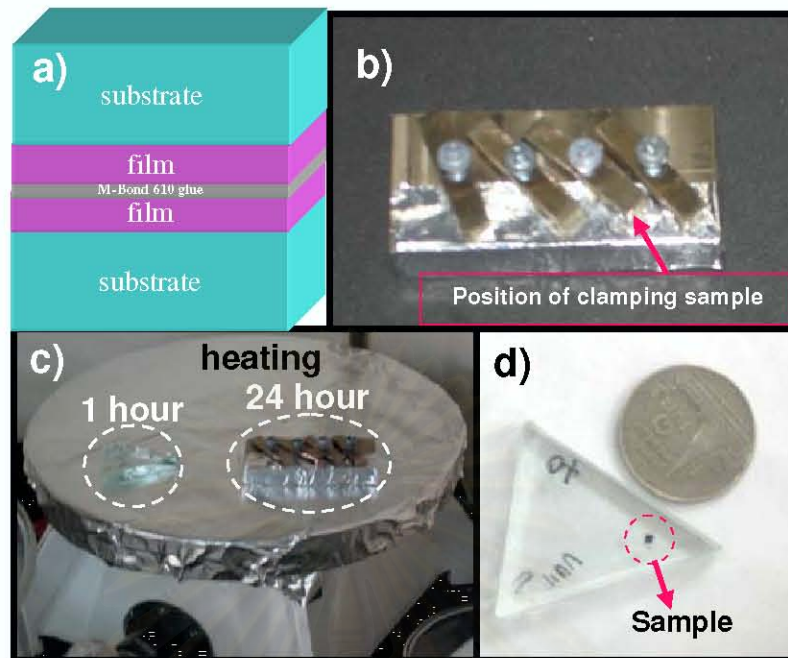


Figure 2.3: a) Schematic diagram of sticking 2 surface samples. b) Clamped sample. c) 80°C heating sample on the hot plate. d) Sample on the triangle holder compared with a coin as in the figure.

Clamping process

The purpose of the clamping process is to keep the sticking surface of 2 samples tight while the polishing process is carried out. Before the surfaces of the cut samples are stuck, they are cleaned by wiping under with acetone and methyl alcohol, respectively. Then, the 2 surfaces of the cut samples are stuck together by M-BOND 610 glue as shown in Fig. 2.3 a). As shown in Fig. 2.3 b), the stuck sample is clamped by a clamping holder. Finally, the stuck samples in the clamping holder are put on a hot plate and heated at temperature about 80°C for 24 hours, as shown in Fig. 2.3 c).

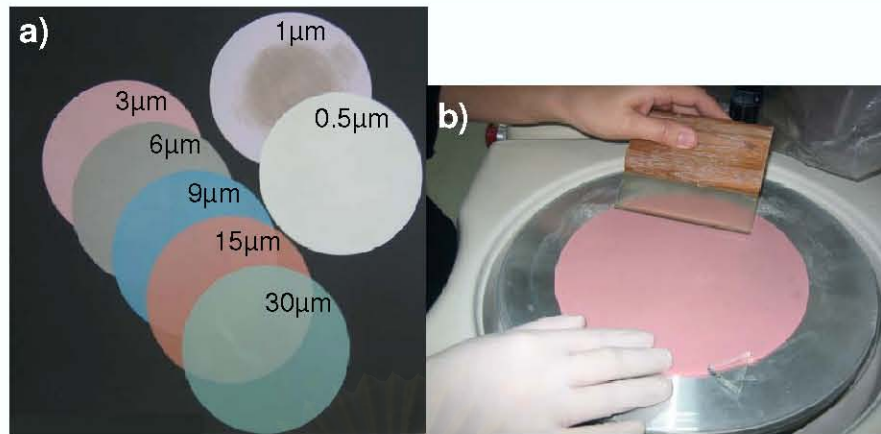


Figure 2.4: a) Diamond films. b) Diamond film on lapping.

Polishing process

The clamped sample is stuck (side-way up) on the polishing holder (triangular-shaped glass) with Kenji glue, as shown in Fig. 2.3 d). To dry the glue, the sample holder is heated on the hot plate at temperature of 80°C for 1 hour (Fig. 2.3 c)). While, a diamond lapping film is attached on the cleaned glass whose diameter is 30 cm as shown in Figure 2.4 b). The sample is polished with diamond lapping films with the diamond grid sizes of 9, 6, 3, 1 and 0.5 micrometer (Fig. 2.4), respectively. The sample is polished until the thickness is approximately a half of its original thickness. The next step, the sample is turned over. Finally, the processes described above are applied to the other surface of the sample until the thickness is approximately 50 μm thick.

Milling process

First, the copper grid is stuck on the polished sample with M-BOND 610 glue. To dry the glue, the sample is heated on the hot plate for 4 hours at temperature of 80°C. Then, the sample on copper grid is taken apart from the polishing holder using acetone. At the last step, the sample on copper grid is milled by Precision Ion Polishing system (PIPs, as shown in Fig. 2.5) (time, voltage and ion beam angle strongly depend on the thickness of sample material). Now, the sample is ready for TEM investigation.



Figure 2.5: Ion beam milling machine.

2.3.2 Plan-view preparation

The plan-view sample is useful for investigation of the micro-(nano-) structural defects in the direction normal to the layer surface. This allows us to characterize the surface morphology, plastic deformation, surface crack, and to get information on the lateral phase distribution. Normal preparation processes of the plan-view sample are the same as those for the preparation of cross-sectional sample. However, the clamping process is not necessary. It is important that the film side of the sample have to be struck on the sample holder and then polished without changing to the other side until the thickness of the sample is approximately $50\ \mu\text{m}$. After that, the milling process is carried out.

Because of the extreme sensitivity of the electron microscope, revealing a detail on a near-atomic scale, the sample preparation techniques for TEM, both cross-sectional and plan-view samples, have to be chosen and prepared with the great care.

2.4 Analytical theory of TEM

TEM analysis is distinctly necessary to use the TEM technique. In general, the TEM analysis is nearly individual for each specimen types such as ceramic, biological cells, bulk materials, heterostructure thin films, etc. In this work, we focus on analysis of semiconducting thin film. To analyze the investigational results, the analytical theory, the crystallography knowledge, and material structure are used. In general, there are two operating modes of TEM. The first one is an image mode which produces TEM micrographs of the specimen with enough details in micro-(nano-)structures. The other is a diffraction mode, which produces diffraction patterns using examination of crystal structure.

2.4.1 Image mode

The image mode is a useful operating mode of TEM because it is used to study the extended defects in micro- to nano- scale, such as dislocation, stacking fault, twin, micro voids, boundaries, etc. The image mode shows results in the form of micrograph generated from the transmitted and diffracted electron beam hitting on phosphor screen. When an electron diffraction (ED) pattern is projected onto the phosphor screen, the ED pattern can be used to perform two basic imaging operations. Normally, the ED pattern contains bright spots which are associated to the direct and scattered electron beams. If the direct beam (central spot) is selected, the resultant image is called “bright-field (BF) image”. On the other hand, if the scattered electron beam is selected, the forming image is called “dark-field (DF) image”. Typical magnification ranges will be in the range of $25,000\times$ - $100,000\times$, depending on adjusting the intermediate lenses of the microscope [23].

The BF and DF images are two basic ways to form an amplitude-contrast in the micrograph. The amplitude contrast (C_A) is defined quantitatively in terms of the different in intensity (ΔI) between two adjacent areas. I_1 and I_2 are intensity of area 1 and area 2, respectively.

$$C_A = \frac{I_1 - I_2}{I_2} = \frac{\Delta I}{I_2}, \quad (2.3)$$

In fact, the contrast in TEM micrograph is seen as different green levels on phosphor screen which are formed by coming electron (transmitting and scattering electrons) from different thickness, structure and crystal orientation of the specimen. If the contrasts in the image were found in some area, it could be primary demonstrated either an appearance of the defects or a difference in orientation of two regions. However, the results must be based on the structural property of material as well as the initial results of previous investigations.

2.4.2 Diffraction mode

The diffraction mode in TEM demonstrates a result in a form of diffraction pattern. The diffraction pattern occurs from the transmitting and diffracting electrons that pass through a thin specimen and then interfere on the phosphor screen as the spots which are called “diffraction spot”. The arrangement of diffraction spot in 2 dimension is called “electron diffraction (ED) pattern”. Therefore, the crystallographic structures (crystal orientation, crystal structure, and lattice parameter) can be deduced by the ED pattern.

Ewald’s sphere construction

In 1913 Peter Ewald has published details of a geometrical construction which has been used ever since to understand the diffraction patterns. When the electron beam hits a crystal plane, Ewald’s sphere shows sets of planes which close to their Bragg angles for diffraction to take place. The incident wave (\vec{k}) incident on a crystal plane as shown in Fig. 2.6.

The crystal plane is represented by its reciprocal lattice \vec{g} , with the origin O. The incident electron beam is represented by a reciprocal vector \vec{k} , ending at the origin O. A circle with radius $1/\lambda$ is constructed, passing through the origin O which indicated by black dotted line. Wherever, a reciprocal point touches the

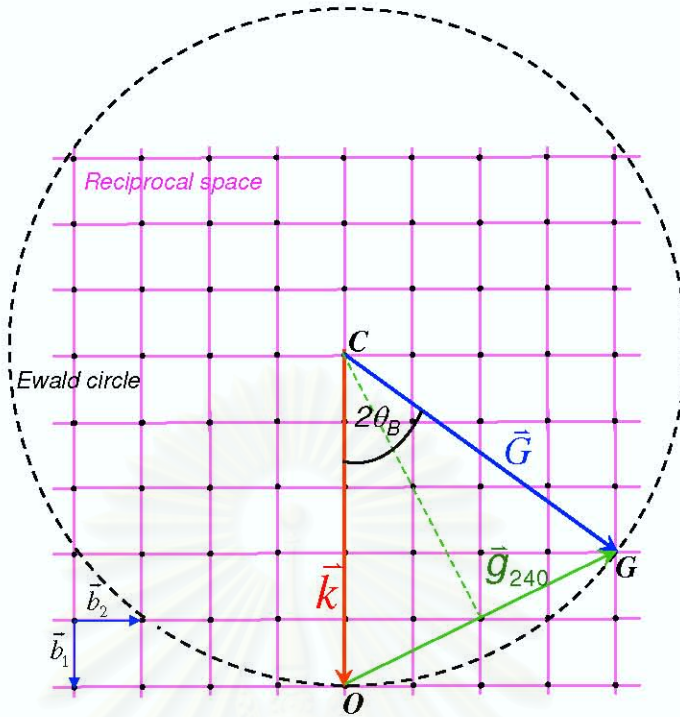


Figure 2.6: The Ewald sphere construction in 2 dimensions. Section through the sphere of the reflection containing the incident beam vector (\vec{k}), the diffracted beam vector (\vec{G}) and reciprocal lattice vector (\vec{g}_{240}), corresponding to $-2\vec{b}_1 + 4\vec{b}_2$ when \vec{b}_1 and \vec{b}_2 are the reciprocal unit vectors [25].

circle, Bragg's law is conformed and the electron diffraction will occur. \vec{CO} stands for the incident electron beam. \vec{CG} represents a diffracted electron beam. The angle between \vec{CO} and \vec{CG} must correspond to the Bragg condition ($2\theta_B$). For example, if \vec{OG} is \vec{g}_{240} , its magnitude will be $1/d_{240}$. Since $|\vec{k}| = 1/\lambda$, thus,

$$\vec{OG} = 2\left(\frac{1}{\lambda}\right)\sin\theta_B = \frac{1}{d_{240}} \quad (2.4)$$

rearranging Eq.2.4, Bragg's equation with $n=1$ will be obtained. In three dimensions, the Ewald circle becomes a sphere and can intersect reciprocal points anywhere in the reciprocal lattice, as shown in Fig. 2.7. In fact, the Ewald sphere can intersect more than one lattice point at the same time. Then, the diffraction pattern which can be recorded for any particular \vec{k} vector is usually seen as a projection onto a two dimension spot on the projecting plane. Whenever the Ewald sphere intersects reciprocal lattice points, the Bragg's equation will be satisfied. Diffraction of electrons will be presented as an ED pattern, representing a recip-

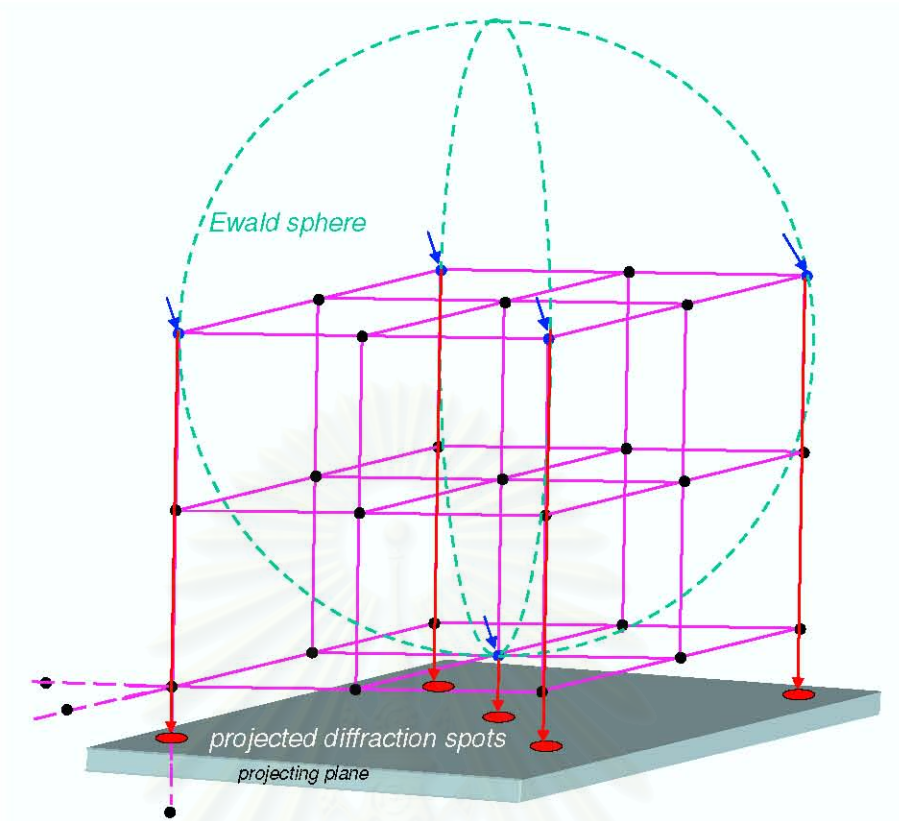


Figure 2.7: Ewald sphere construction in 3 dimensions and the projection of intersected points on the projecting plane as a diffraction spots. The intersected points are indicated by arrows.

reciprocal lattice in 2 dimensions on any zone axis. Therefore, the understanding in reciprocal space is distinctly necessary to interpret the obtained results.

Reciprocal space

Due to the reciprocal lattice corresponding to the real crystal lattice, the vectors \vec{a}_1 , \vec{a}_2 and \vec{a}_3 are defined as the unit vectors of the crystal lattice, corresponding to reciprocal lattice vectors, \vec{b}_1 , \vec{b}_2 and \vec{b}_3 , as following

$$\vec{b}_1 = \frac{1}{V}(\vec{a}_2 \times \vec{a}_3) \quad (2.5)$$

$$\vec{b}_2 = \frac{1}{V}(\vec{a}_3 \times \vec{a}_1) \quad (2.6)$$

$$\vec{b}_3 = \frac{1}{V}(\vec{a}_1 \times \vec{a}_2) \quad (2.7)$$

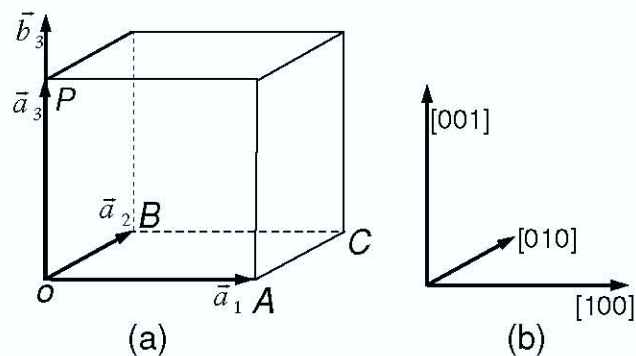


Figure 2.8: (a) Location of the reciprocal-lattice axis b_3 (b) $[hkl]$ direction in the reciprocal lattice [25].

where, V is the volume of the crystal unit cell. The vectors \vec{b}_1 , \vec{b}_2 and \vec{b}_3 are defined in terms of the vectors \vec{a}_1 , \vec{a}_2 and \vec{a}_3 . This relation is useful for structural investigation of crystal structures. Consider the conventional cubic unit cell, as shown in Fig. 2.8, the reciprocal lattice vector \vec{b}_3 is perpendicular to the plane of \vec{a}_1 and \vec{a}_2 . Since OP (the projection of \vec{a}_3 on \vec{b}_3) is equal to the height of the unit cell, perpendicular to the (001) planes of the crystal lattice, the length of $|\vec{b}_3|$ is given by

$$|\vec{b}_3| = \frac{1}{V}(\vec{a}_1 \times \vec{a}_2) = \frac{\text{area of } OACB}{(\text{area of } OACB)(\text{height of cell})} = \frac{1}{OP} = \frac{1}{d_{001}} \quad (2.8)$$

Similarly $|\vec{b}_3|$, the reciprocal lattice axes, \vec{b}_1 and \vec{b}_2 , are normal to the (100) and (010) planes of the crystal lattice, respectively. Their magnitudes are equal to the reciprocals of the spacings of (100) and (010) planes. Figure 2.9 shows illustration of the reciprocal lattice corresponding to the real plane in the conventional unit cells. This produces an array of the points which are labeled by their coordinates in terms of the planes (200) , (020) , (002) and (111) .

Furthermore, Fig.2.10 shows an extension of the reciprocal lattice in 3 dimensions (3D). If the 3D reciprocal lattice is seen along the $[002]$ direction, the 2 dimensions (2D) reciprocal lattice will be presented in Fig.2.11. The 2D reciprocal lattice is also a diffraction pattern of fcc structure along the $[002]$ zone axis in TEM diffraction mode.

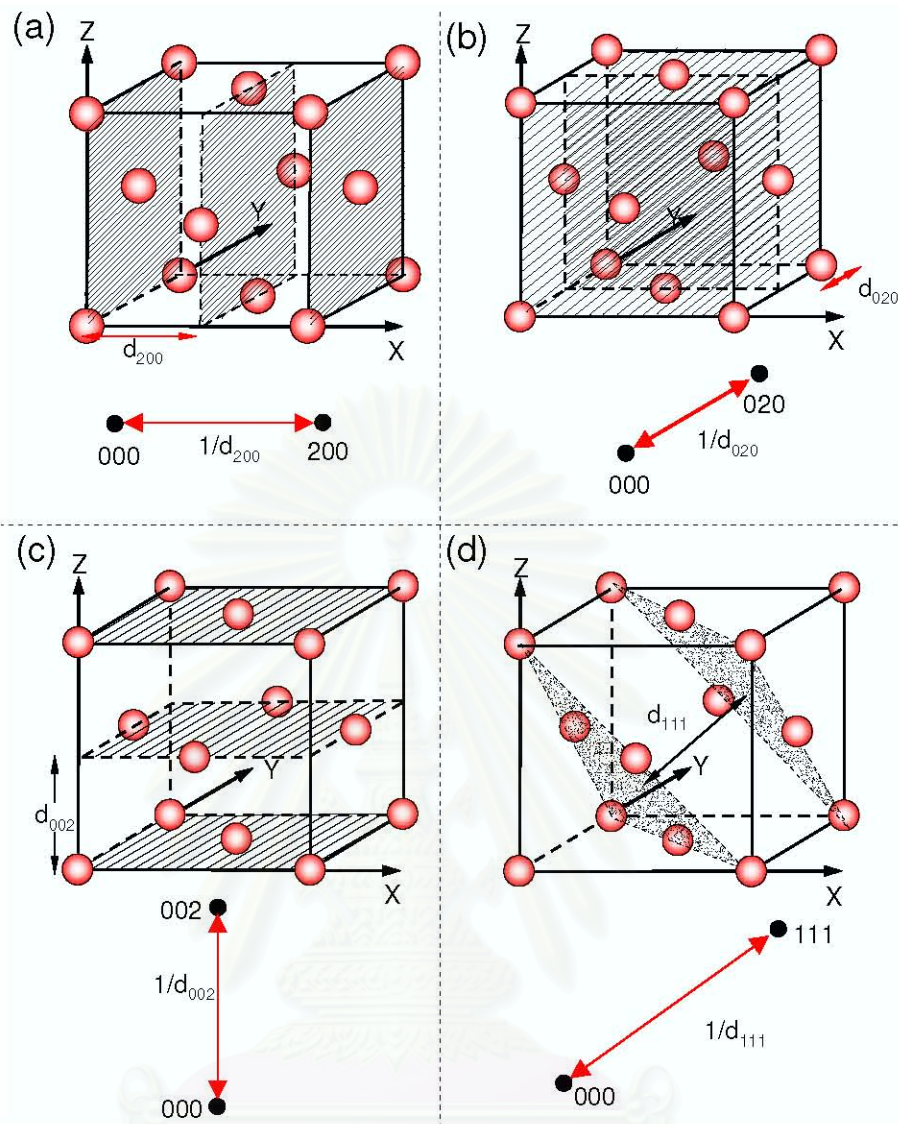


Figure 2.9: Schematic illustration of (a) (200), (b) (020), (c) (002) and (d) (111) planes in the fcc unit cell and the corresponding reciprocal lattice points

Indexing the diffraction spots

The diffraction spots are formed by the transmitting and diffracting electron beams in TEM, as shown in Fig. 2.12. The incident electron beam (I) is scattered by a crystal lattice inside the specimen. The direct transmitted beam (T) and the diffracted beam (D) can be found in a diffraction pattern. Besides, there are other scattering directions (N) that their intensity does not appear. The ED pattern is known as any two dimensions of a reciprocal lattice. For example, in Fig. 2.13, the ED pattern taken from a cubic phase on a (110) cross-section (along [110])

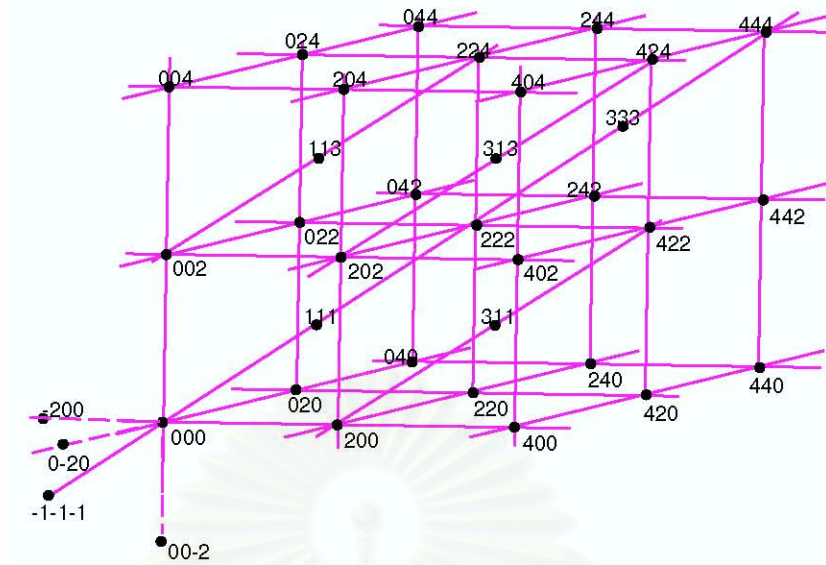


Figure 2.10: A sector of the full fcc reciprocal lattice (3-D). The other sectors can be imagined extending in the directions of the dotted lines.

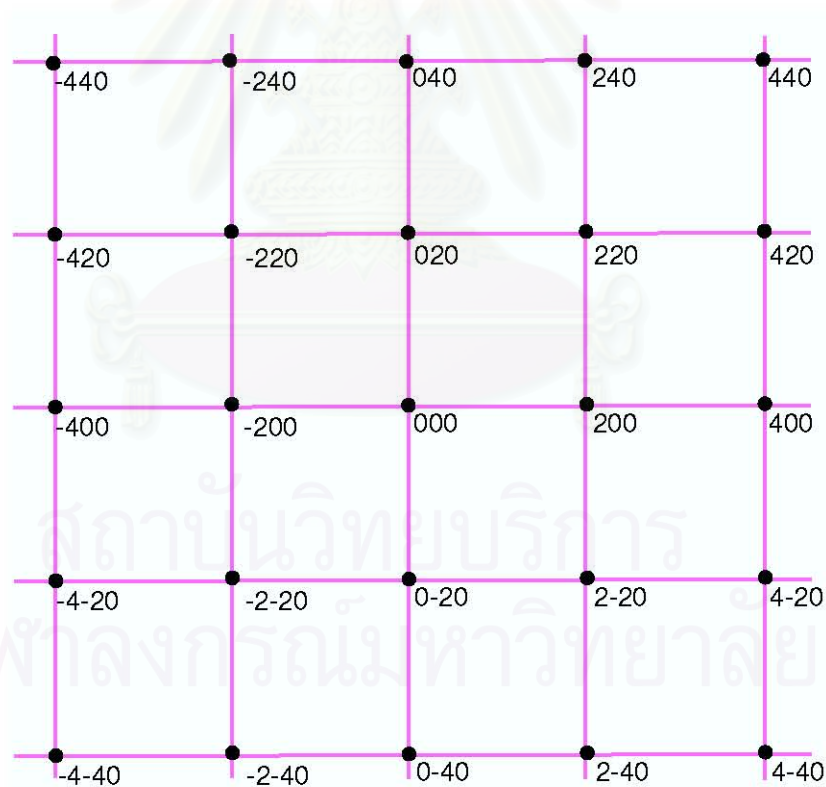


Figure 2.11: $[002]$ Reciprocal lattice section (2-D) taken from the full reciprocal lattice.

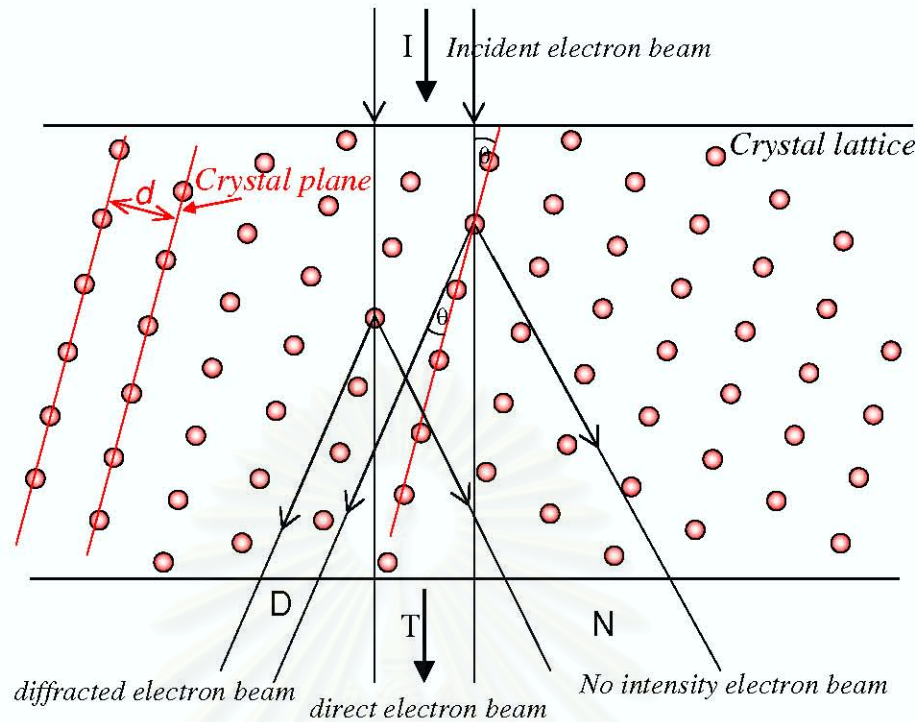


Figure 2.12: The scattering of an incident electron beam (I) by a crystal lattice. In other side of specimen, two kinds of intense beam can be found: the direct beam (T) and the diffracted beam (D). In other directions (N) no intense electron beam will be detected.

zone axis) is shown. Fundamentally, we only use 2 spots to index plane which are indicated as A and B spots, as shown in Fig. 2.13. The one biggest spot (spot O) is chosen as an origin. This spot corresponds to the direct transmitted beam (T) which is parallel to the zone axis. Then, we measure a magnitude of 2 reciprocal vectors (\vec{R}_A and \vec{R}_B) as shown in Fig. 2.13, while all others can be deduced by vector addition. θ which is an angle between the reciprocal vectors \vec{R}_A and \vec{R}_B is measured.

In this case, we can determine the crystal structure to be a cubic structure. The lattice parameter for the cubic structure can be determined by

$$d = \frac{a}{\sqrt{h^2 + k^2 + l^2}} \quad (2.9)$$

d is the interplanar spacing in the crystal along the $[hkl]$ direction. In addition,

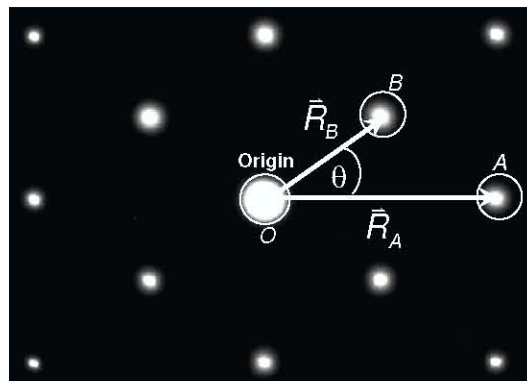


Figure 2.13: Diffraction pattern of GaN along [110] zone axis.

the elastically scattered electrons satisfy Bragg condition as followed

$$2d\sin\theta = n\lambda \quad (2.10)$$

where λ is wavelength of the electrons, θ is the Bragg angle and n can be any integer. In electron diffraction, only first order diffraction, i.e. $n=1$, is considered and higher order diffraction is simply dealt with by using multiples of the miller indices. Typically, the Bragg angle θ is very small (less than 10 radians). Thus, $\sin\theta$ can be approximated by θ . Hence, the Bragg equation can be rewritten as

$$2d\theta = \lambda \quad (2.11)$$

Figure 2.14 is a schematic diagram showing the formation of an ED pattern on the main phosphor screen. For a small diffracted angle, $R/L = 2\theta$. Combining with the Eq. 2.11, we get

$$\frac{R}{L} = \frac{\lambda}{d} \quad (2.12)$$

or

$$Rd = L\lambda \quad (2.13)$$

The quantity $L\lambda$ is called “camera constant”, since it is independent of the specimen. Using d from Eq. 2.9, Eq. 2.13 becomes

$$\frac{L\lambda}{R} = \frac{a}{\sqrt{h^2 + k^2 + l^2}} \quad (2.14)$$

The L , λ and a are constant values for the camera length, the electron wavelength and the lattice parameter, respectively. In Fig. 2.13, if R_A is divided by R_B , we

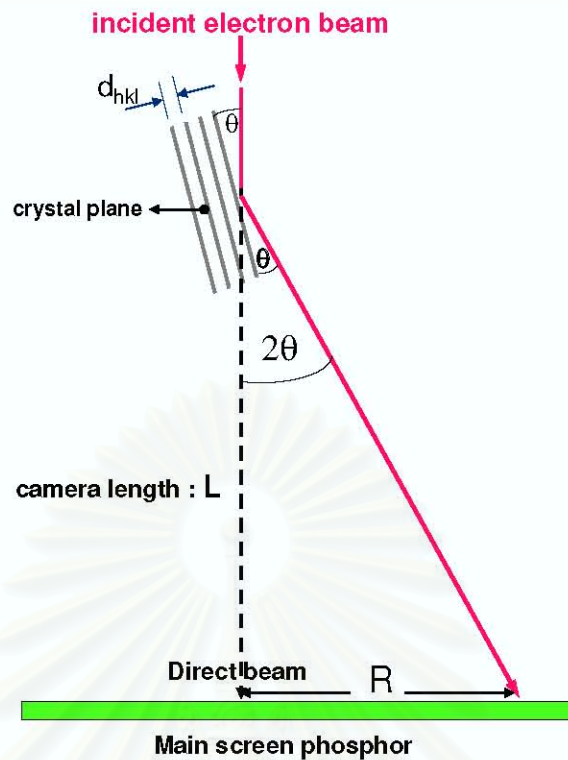


Figure 2.14: Schematic illustration of electron diffraction in TEM [28]

will get the ratio of the reciprocal lattice spacing of any zone axis as following

$$\frac{R_A}{R_B} = \frac{\sqrt{h_A^2 + k_A^2 + l_A^2}}{\sqrt{h_B^2 + k_B^2 + l_B^2}} \quad (2.15)$$

The next step, we should prepare a table giving the ratios of the spacings of permitted diffraction planes in the known structure. In this work, we focus on the fcc structure. Therefore, the known spacing ratios taken for the fcc structure were determined and shown in Table 2.1.

Finally, the measured ratio R_A/R_B are taken and then compared with those in Table 2.1. Thus, the miller indices of these two spots will be obtained. For example, the R_A/R_B ratio determined from the measurements of ED pattern in Fig. 2.13 is about 1.63. The spacing ratio shown in Table 2.1 indicates that the A spot and B spot correspond to $\{220\}$ and $\{111\}$ planes, respectively. To confirm these results, the angle between both planes, which have been indexed, is examined using the scalar product, as following

$$\vec{a} \cdot \vec{b} = ab \cos \theta \quad (2.16)$$

		R_A					
R_B	hkl	{111}	{200}	{220}	{311}	{222}	{400}
	{111}	1	1.16	1.63	1.91	2	2.31
	{200}	0.87	1	1.41	1.66	2.45	2.83
	{220}	0.61	0.71	1	1.17	1.22	1.41
	{311}	0.52	0.60	0.85	1	1.04	1.21
	{222}	0.50	0.58	0.82	0.96	1	1.15
	{400}	0.43	0.50	0.71	0.83	0.87	1

Table 2.1: The spacing ratios of some planes for fcc structure.

so, for [220] and [111] vectors

$$[220] \cdot [111] = |[220]| \times |[111]| \cos \theta \quad (2.17)$$

and check with the measured angle, θ in Figure 2.13. If the measured angle agrees with the calculated angle, the indexing will be accepted. In this case, the measured θ is 35.2 degree, while the calculated θ is 35.26 degree. It confirms the results of indexing. To complete indexing, the orientations of sample from the growth must be used. Moreover, if the camera length and the measured spacing R are known, then the lattice parameter a can be determined using the angle approximation method, Eq. 2.13 and Eq. 2.9. In addition, if the electron beam are diffracted from a high quality crystal plane (perfectly parallel plane) in real space, the diffracted spots will be formed as a single round spot. On the other hand, the spot with streak is formed by the diffracted electron beam from low quality crystal plane (unparalleled plane) which might corresponds to the formation of some planar defects.

CHAPTER III

STRUCTURAL DEFECTS IN *c*-GaN FILM

In this chapter, we describe the investigational results of the *c*-GaN film grown on GaAs (001) substrate using scanning electron microscopy (SEM), x-ray diffraction (XRD) and transmission electron microscopy (TEM). The main structural defect in the *c*-GaN film is examined to be planar defects (stacking fault and twin). In addition, an atomic model is also used to describe the formation mechanism of such planar defects in microscopic scale.

3.1 Initial investigated results of *c*-GaN film

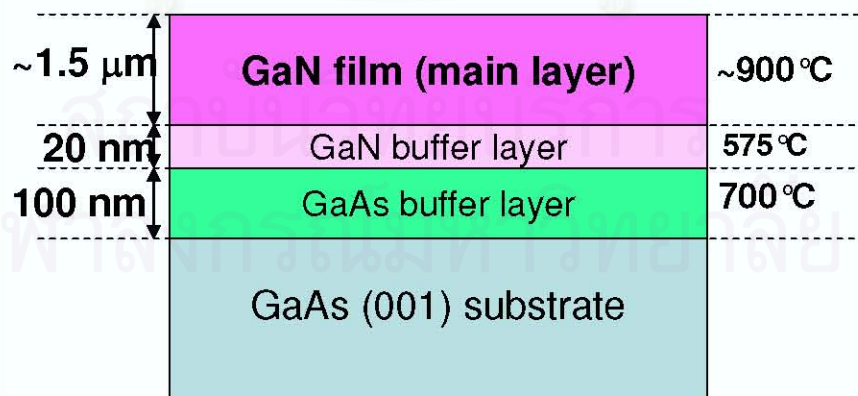


Figure 3.1: Schematic illustration of the GaN layer grown on a GaAs (001) substrate.

In this part, initial investigated results of *c*-GaN grown film, such as surface morphology and crystal structures, are discussed. In this study, the investigated *c*-GaN film was grown on the GaAs (001) substrate by metalorganic vapor phase epitaxy (MOVPE) using trimethylgallium (TMGa), dimethylhydrazine (DMHy) and Arsine (AsH₃), as the source materials of Ga, N and As, respectively. The detailed sample structure is shown schematically in Fig. 3.1.

To prevent the surface roughening of the GaAs substrate, the growth was initially started on the GaAs (001) substrate with a 100 nm-thick GaAs buffer layer at 700°C. For the GaAs buffer layer, the V/III ([AsH₃]/[TMGa]) ratio was fixed to be 100. Then the temperature was reduced and stabilized at 575°C for the growth of a 20 nm-thick *c*-GaN buffer layer. Finally, a *c*-GaN main layer was grown at growth temperature of about 900°C. The V/III ([DMHy]/[TMGa]) for the *c*-GaN buffer and main layers were 100 and 25, respectively. The thickness of the *c*-GaN main layer was determined to be about 1.5 μm. An overview of structural properties (morphology and crystal structures) of the MOVPE grown *c*-GaN film was obtained by SEM and XRD measurements.

3.1.1 Surface morphology of *c*-GaN film

Figure 3.2 shows cross-sectional SEM image of the MOVPE grown *c*-GaN film on GaAs (001) substrate. It is clearly seen in the Figure that the thickness of *c*-GaN layer is about 1.5 μm. Many micro-voids were observed at the GaN/GaAs interface. The reason for occurrence of the micro-voids is considered to be the desorption of surface atoms at high growth temperature (900°C). The situation is similar for the GaP substrate [26]. Even though, the *c*-GaN surface is mirror-like to the eye, its SEM image shows rough surface morphology with triangular domains. In addition, the patterned roughness on the surface of the film is noticeably observed. Continuity of the striped roughness pattern from the (001) surface to (110) cross-section of the *c*-GaN is clearly seen as indicated by dashed red-line. This indicates that some planar defects may have incorporated in the *c*-GaN layer.

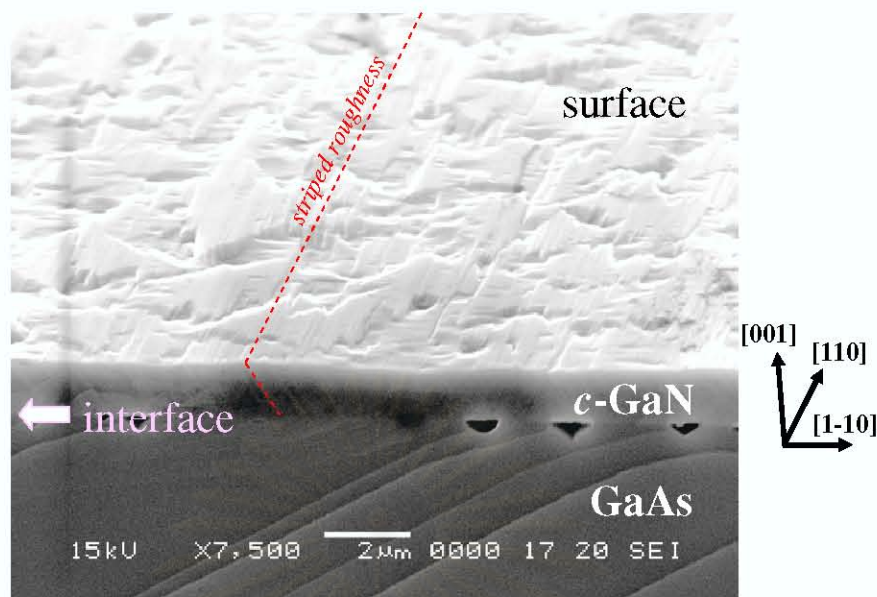


Figure 3.2: SEM cross-sectional micrograph and surface morphology of GaN epitaxial layer on GaAs substrate at growth temperature $\sim 900^\circ\text{C}$.

3.1.2 Crystal structure of *c*-GaN grown film

In x-ray diffraction (XRD) measurements, the most frequently used scan mode is $2\theta/\omega$ scan. For an epitaxial film, only the plane spacings parallel to the film surface are usually measurements. Figure 3.3 shows $2\theta/\omega$ XRD profile using CuK_α radiation for the *c*-GaN film grown on GaAs (001) substrate at growth temperature of 900°C . The cubic (002) diffraction is clearly observed, whereas the hexagonal (0002) diffraction is absent. It clearly demonstrates that the grown film has a cubic structure. From the *c*-GaN (002) diffraction, the lattice constant of *c*-GaN (a_{cub}) was calculated to be 4.51 \AA . It can be also theoretically calculated from that of hexagonal phase GaN (a_{hex}); $a_{\text{cub}} = \sqrt{2}a_{\text{hex}}$. Taking $a_{\text{hex}} = 3.189 \text{ \AA}$ [27], a_{cub} is calculated to be 4.51 \AA . This is in good agreement with our experiment. It shows that the *c*-GaN film is relaxed and almost free strain. It is therefore seen that although the *c*-GaN film has a large mismatch with the GaAs substrate ($20\cdot/\cdot$), it is almost relaxed at the early stage of the GaN growth.

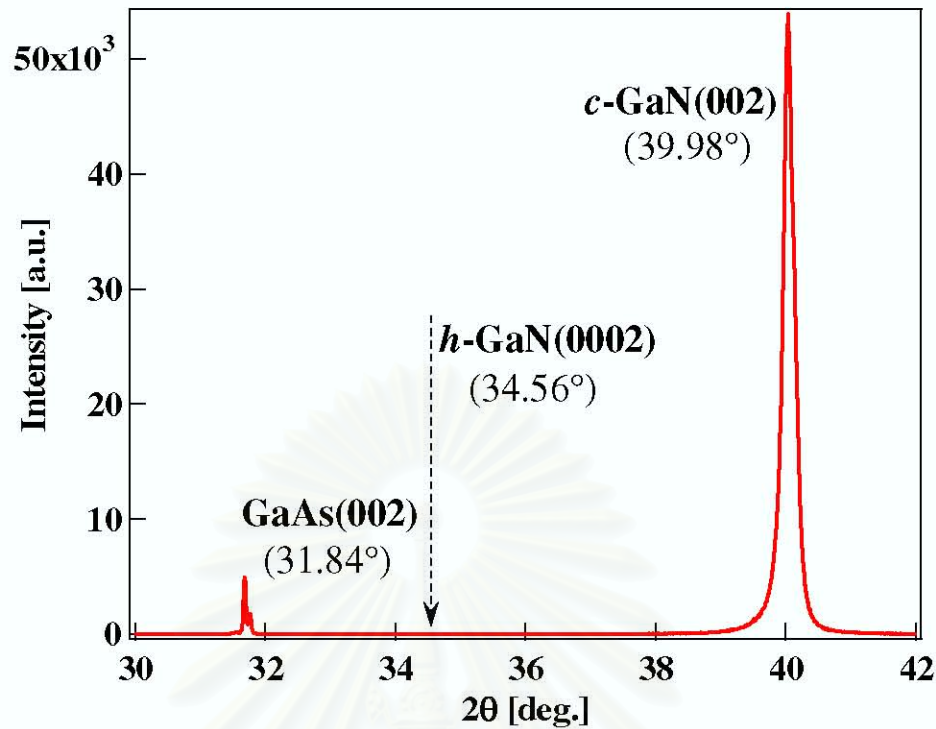


Figure 3.3: X-ray diffraction profiles of GaN film grown at 900°C on GaAs (001) substrate.

3.2 TEM investigations of *c*-GaN film

In this section, transmission electron microscopy (TEM) was used to investigate the micro-(nano-)structural defects in *c*-GaN layer on GaAs (001) substrate. The specimen of *c*-GaN was sliced by a diamond cutting saw to a thickness of about 1 mm in the direction perpendicular to the [-1-10] direction, being parallel to the (110) plane. The sliced specimen was mechanically polished down to about 0.05 mm and was finally etched by argon ion milling (GATAN PIPS model 691). Observation was carried out using a JEM-2000EX microscope operating at 200 kV. Projected potential micrographs were obtained to discuss the micro-(nano-)structure of *c*-GaN film. Figure 3.4 shows a) a bright-field (BF) cross-sectional TEM micrograph and b) an electron diffraction (ED) pattern of the *c*-GaN film on GaAs substrate. One can see that the ED pattern consists of spots which are round and streaking, being for GaAs and GaN, respectively. The positions of the diffraction spots from GaN reveal that the GaN has a cubic structure, or *c*-GaN,

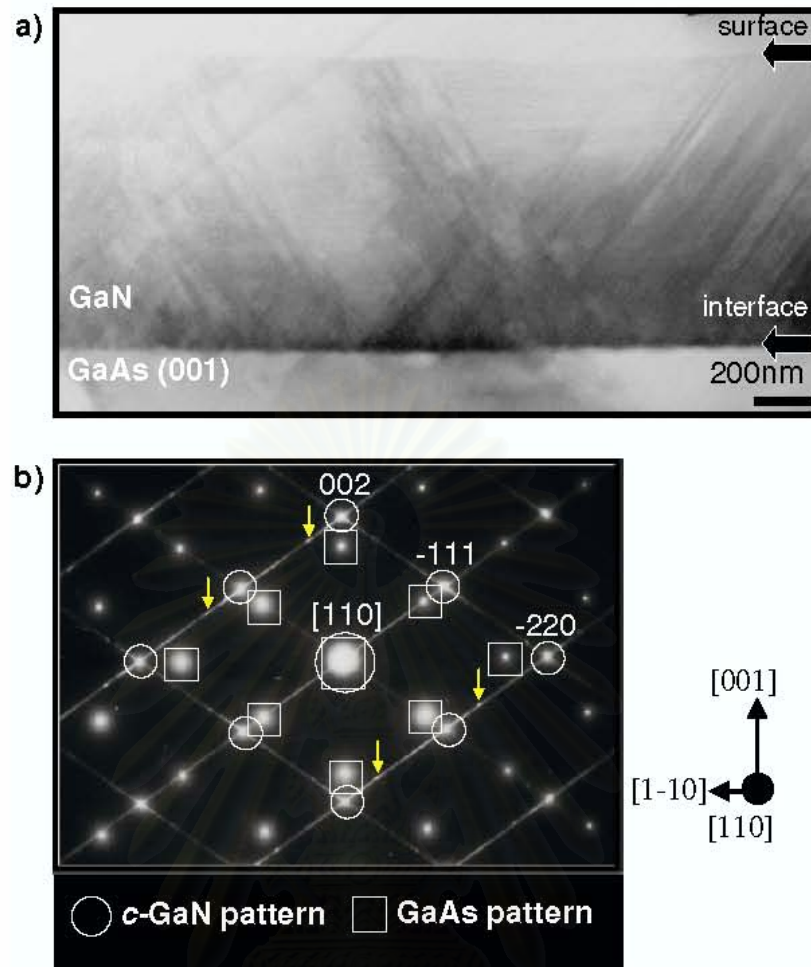


Figure 3.4: TEM results of GaN film and GaAs substrate region at growth temperature $\sim 900^\circ\text{C}$ a) Cross-sectional micrograph. b) Electron diffraction (ED) patterns.

which has the same orientation as the GaAs substrate ($c\text{-GaN}(001)//\text{GaAs}(001)$ and $c\text{-GaN}[110]//\text{GaAs}[110]$). The streaks demonstrate the existence of planar defects such as stacking faults (SFs) and twins on (111) planes. It is noted that the intensity distribution of the streaks (Fig. 3.4 b)) is not symmetric with respect to the primary diffraction spots. The asymmetry implies that SFs are not randomly inserted but occur with some regularity. The streaks have small intensity maxima at the position marked by arrows, suggesting that the regions with SFs tend to have a hexagonal stacking sequence, i. e., a hexagonal structure or $h\text{-GaN}$. The BF cross-sectional TEM micrograph shows distinct contrasts, which are inclined at about 54.7° to the GaAs (001) plane. This means that the contrasts, which

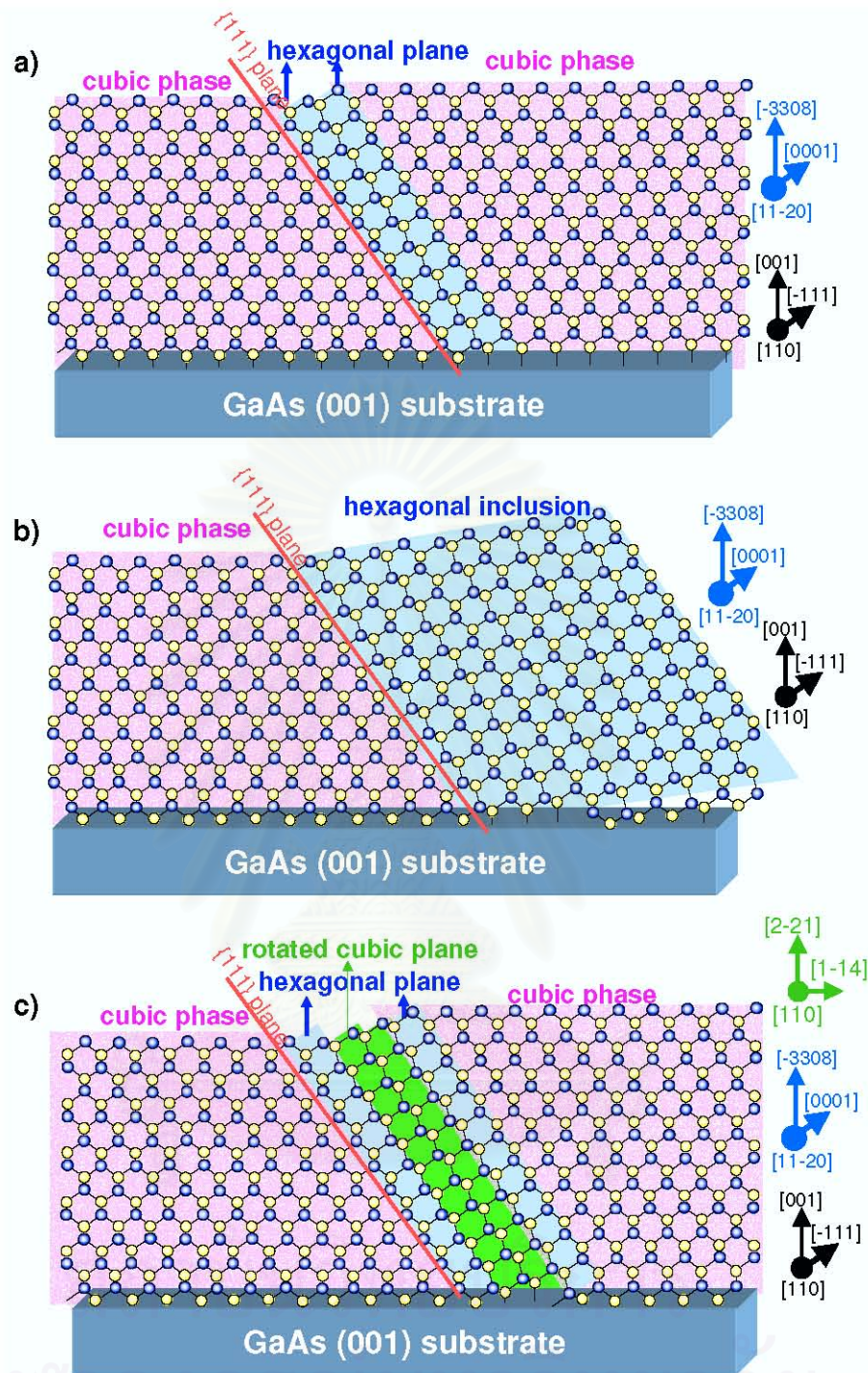


Figure 3.5: Illustrations of possible crystal defects in the *c*-GaN film at the (110) cross-section a) Stacking fault b) Hexagonal inclusion c) Twin.

are nearly parallel to $\{111\}$ in *c*-GaN, are due to SFs as well as twins. One can see that these planar defects often interact with each other and then stop their propagation within the layer. A part of the stacking faults, however, extends

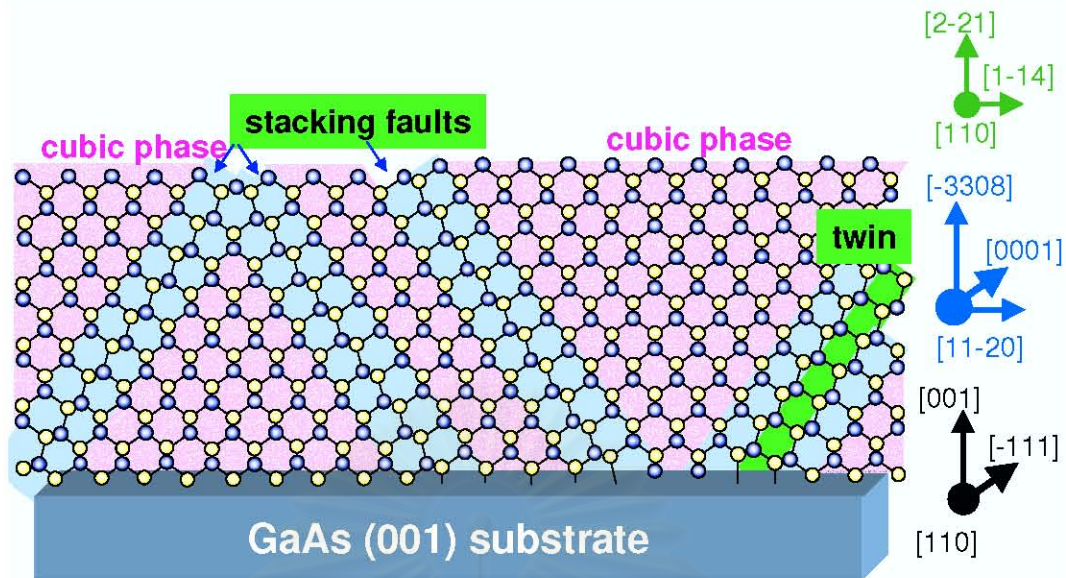


Figure 3.6: Illustration of planar defects (stacking fault and twin) in the *c*-GaN film on GaAs substrate at growth temperature $\sim 900^\circ\text{C}$ at the (110) cross-section

throughout the whole epilayer. A schematic diagram of the possible planar defect formations along (111) cubic planes, which are stacking fault, hexagonal inclusion and twin, is shown in Fig. 3.5. Due to the structural similarities between *c*-GaN (111) and *h*-GaN (0001) surfaces, they are general stacking faults with respect to each other. Commonly, as shown in Fig. 3.5 a), the SF in the *c*-GaN (111) is an insertion of 1 or 2 mono-layers (MLs) of the hexagonal structure. On the other hand, if an inclusion of *h*-GaN is generated in the *c*-GaN layer, then the single crystal *h*-GaN regions constructed along the *c*-GaN (111) surfaces (in Fig. 3.5 b)), should be observed. Figure 3.5 c) illustrates a schematic view of twin defects generated in the *c*-GaN layer. Figure 3.6 shows structural defects in the *c*-GaN film on GaAs substrate at growth temperature $\sim 900^\circ\text{C}$. In fact, no indication of the inclusion of single crystal *h*-GaN was found. Thus, these structural defects should be the SF and twins as shown in Fig. 3.6.

3.3 Summary

From the cross-sectional TEM observation of the GaN layer grown by MOVPE on GaAs (001) substrate, the following results concerning the micro-(nano-) structure of GaN were obtained.

(1) The GaN grown layer has a cubic structure (*c*-GaN) with an epitaxial orientation relationship with the GaAs (001) substrate.

(2) The microstructure is characterized by a high density of planar defects, namely SFs and twins, close to the *c*-GaN/GaAs interface, which results in streaking of diffraction spots on the ED pattern. The SF-region in *c*-GaN layer tends to have a 2H-like-structure, i.e., a hexagonal structure or *h*-GaN.

(3) The lattice of *c*-GaN is almost strain-relieved. Based on the XRD results, the lattice parameter of *c*-GaN was calculated to be $a_{cub} = 4.51 \text{ \AA}$.

(4) No indication of hexagonal phase inclusion was observed.

Finally, we have demonstrated that the main structural defects in the *c*-GaN grown layer are SF and twin defects.

CHAPTER IV

GENERATION OF *h*-GaN IN *c*-GaN

In this chapter, the generation of hexagonal phase GaN (*h*-GaN) in *c*-GaN films is described from the viewpoint of crystal structure control. The effect of growth temperature in the MOVPE grown *c*-GaN films has been investigated. It is found that the polytype transition of GaN from cubic to hexagonal phases is greatly dependent on the growth temperature. Finally, the influence of growth temperature on the generation of planar defects (stacking faults and twins) and single phase *h*-GaN in the *c*-GaN films is also discussed.

4.1 Initial investigated results of *c*-GaN films

In this study, the *c*-GaN layers were grown on semi-insulating (SI) GaAs (001) substrates at temperature ranging from 900 to 960°C by metalorganic vapor phase epitaxy (MOVPE), which has been described elsewhere [15, 29]. Figure 4.1 shows schematic illustration of the GaN grown film at growth temperatures of 900 to 960°C. Trimethylgallium (TMGa) and 1,1-dimethylhydrazine (DMHy) were used as the precursors of Ga and N, respectively. The *c*-GaN films were grown using a two-step growth process. An about 100 nm thick GaAs buffer layer was firstly grown at 700°C, followed a 20 nm thick *c*-GaN buffer layer at 575°C with a V/III ratio of 100. Then an about 1.5 μm thick *c*-GaN film was grown at 900-960°C with a V/III ratio of 25. The growth rate was 6 $\mu\text{m}/\text{h}$ determined by the TMGa molar flow rate of 18 $\mu\text{mol}/\text{min}$.

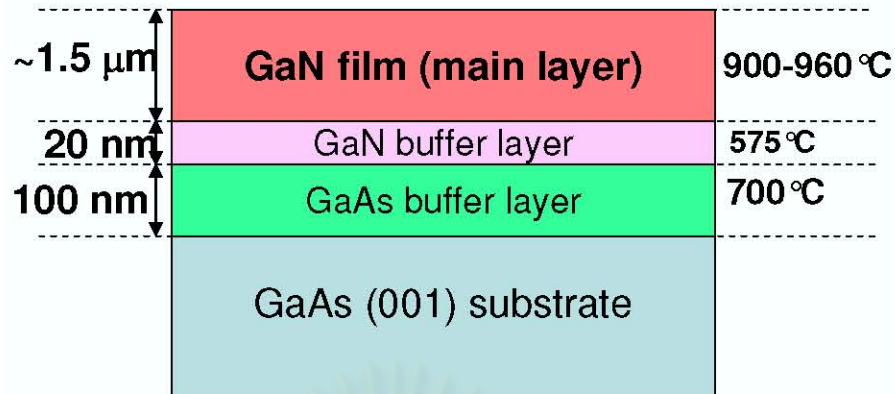


Figure 4.1: Schematic illustration of the GaN layer grown on a GaAs (001) at growth temperature of 960 $^{\circ}\text{C}$

Structural and optical properties of *c*-GaN films were investigated by XRD, TEM and photoluminescence (PL) respectively. The TEM specimens were sliced by a diamond cutting saw to a thickness of 1 *mm* in the direction parallel to (1-10) plane. The sliced platelet specimen was mechanically polished down to 0.01 *mm* and was finally etched by argon ion milling (GATAN PIPS model 691).

4.1.1 Effect of growth temperature on crystal structure

X-ray diffraction (XRD) was primarily used to characterize the structural quality of the MOVPE grown *c*-GaN films on GaAs (001) substrates at different growth temperatures (900 and 960 $^{\circ}\text{C}$). It indicates that all *c*-GaN films condensed in cubic phase. As shown in Fig. 4.2, the diffraction peaks of *c*-GaN were clearly observed at 39.98 $^{\circ}$. On the other hand, no diffractions were observed at 34.56 $^{\circ}$ and 36.84 $^{\circ}$ where *h*-GaN would give the (0002) and the (1-101) diffractions, respectively. Full-width-at-half-maximum (FWHM) of ω -scan for the *c*-GaN (002) plane was increased from 30.0 *arcmin* to 40.4 *arcmin* with increasing growth temperature from 900 $^{\circ}\text{C}$ up to 960 $^{\circ}\text{C}$. In order to investigate the effect of growth temperature on the generation of hexagonal phase in *c*-GaN films, the volume amount of hexagonal phase inclusion is estimated from the ratio of the integrated XRD intensities of the cubic (002) and hexagonal (1-101) planes measured by the ω -scan. It demonstrates that the hexagonal phase inclusion is heavily dependent

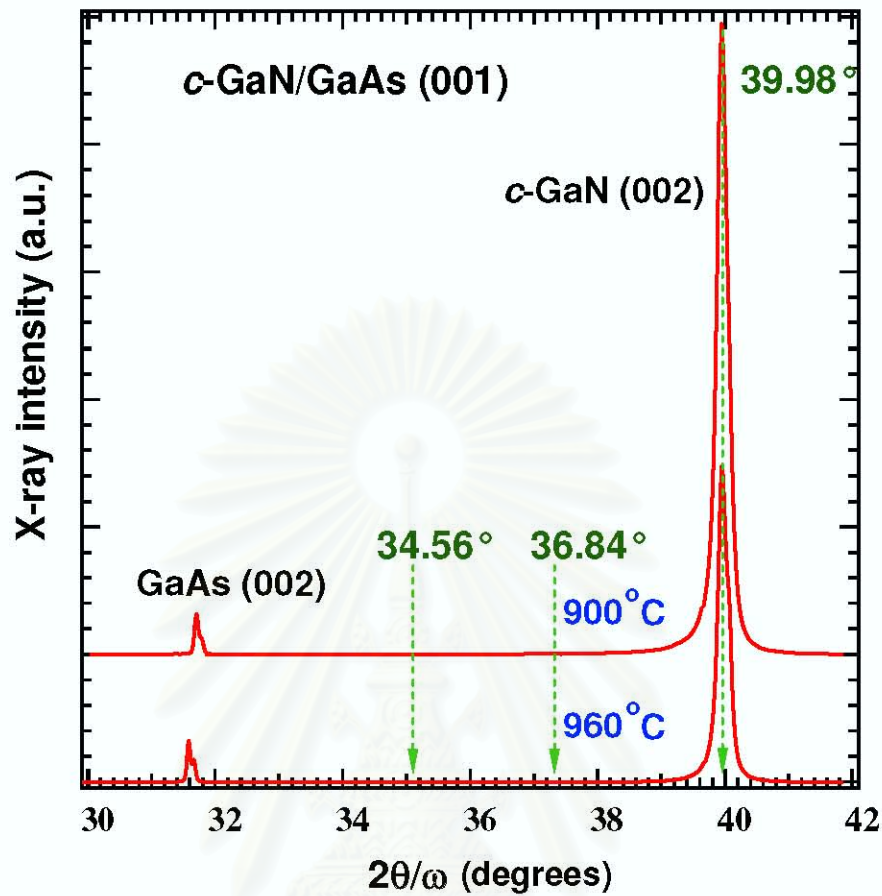


Figure 4.2: $2\theta/\omega$ -scan XRD (002) profiles of *c*-GaN films grown at different growth temperatures of 900°C and 960°C

on the growth temperature. In fact, the cubic phase purity higher than 85 percent was achieved for the *c*-GaN film grown at 900°C [30]. With increasing the growth temperature up to 960°C, the hexagonal phase inclusion in such high-temperature grown *c*-GaN film is relatively higher (>40 percent) than that in *c*-GaN film grown at 900°C (<15 percent) [30].

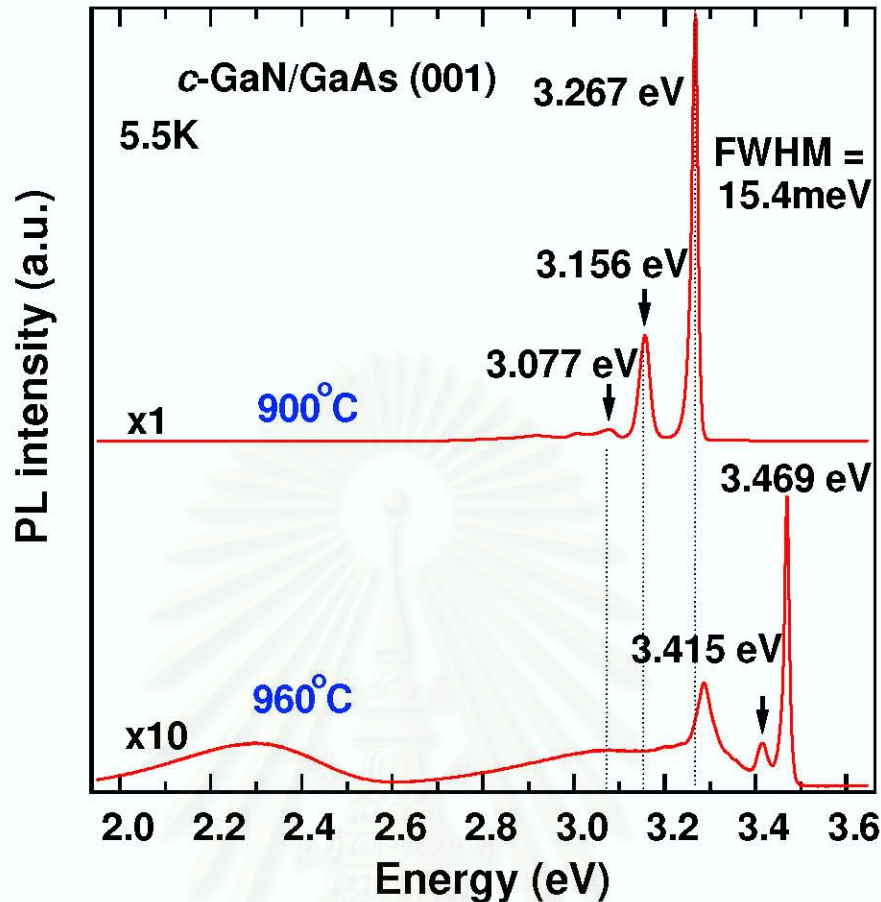


Figure 4.3: Low-temperature (5.5 K) PL spectra of the corresponding *c*-GaN films at different growth temperatures of 900°C and 960°C.

4.1.2 Correlation between luminescence properties and crystal structure

Figure 4.3 shows the low-temperature (5.5 K) PL spectra of the *c*-GaN films grown at temperatures of 900 and 960°C. For the 900°C grown layer, the PL spectrum consists of excitonic emission of *c*-GaN at 3.267 eV with FWHM of 15 meV. The donor-acceptor (D-A) pair recombination around 3.156 eV is very weak. It is also clearly seen in the figure that the other luminescence peaks at around 3.415 and 3.469 eV corresponding to the emission of *h*-GaN are not observed. It is also noticeable that the orange luminescence observed at 2.05 eV [31] is hardly observed from this *c*-GaN film. As the growth temperature rises, the

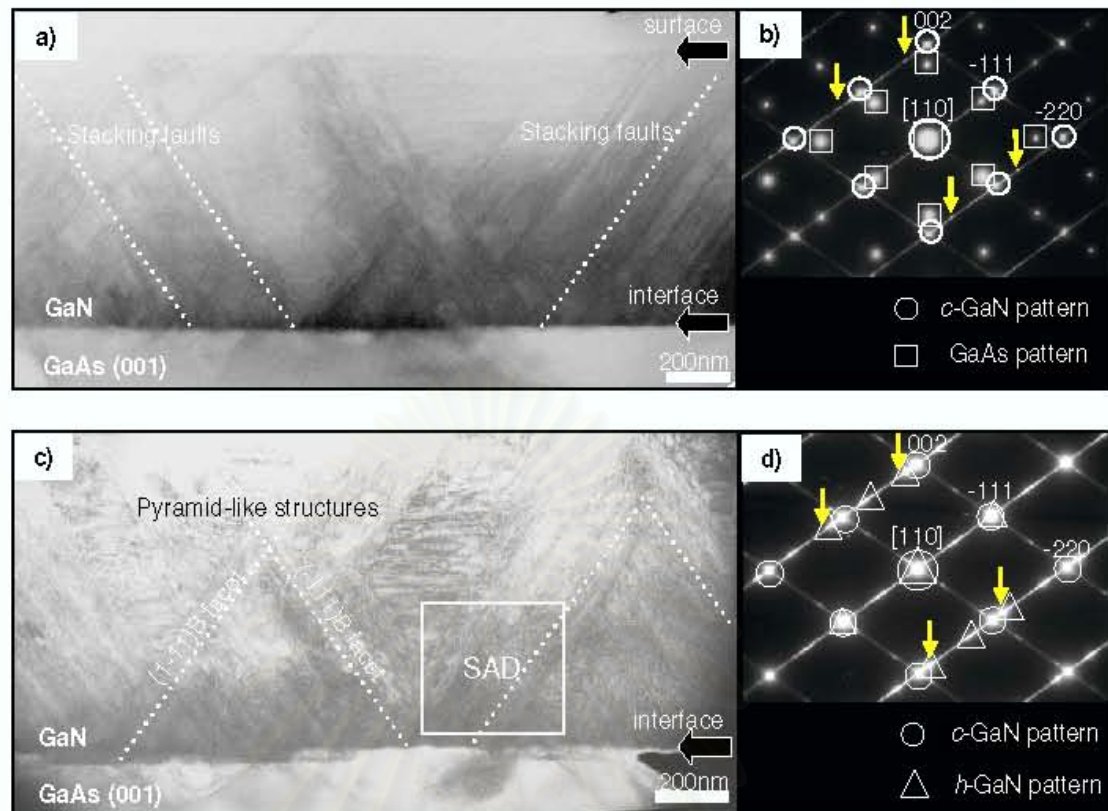


Figure 4.4: Cross-sectional TEM micrographs for the *c*-GaN layers grown on GaAs(001) substrates at different growth temperatures of a) 900°C and c) 960°C. b) and d) Corresponding selected area diffraction (SAD) patterns taken near the $\langle 110 \rangle$ zone axis.

hexagonal peak of GaN at 3.469 eV becomes stronger while the cubic peak (3.267 eV) becomes weaker. In addition, the yellow luminescence peak of *h*-GaN at ~ 2.2 eV is clearly seen. The difference in the PL spectra is in connection with the different amount of hexagonal phase inclusion in the *c*-GaN films, which agrees well with the results of XRD.

4.2 TEM investigations of *c*-GaN films

To understand the above results, the *c*-GaN films were studied by cross-section TEM and selected area diffraction (SAD). The bright-field (BF) TEM micrographs and the SAD patterns in Fig. 4.4 represent the *c*-GaN films grown on

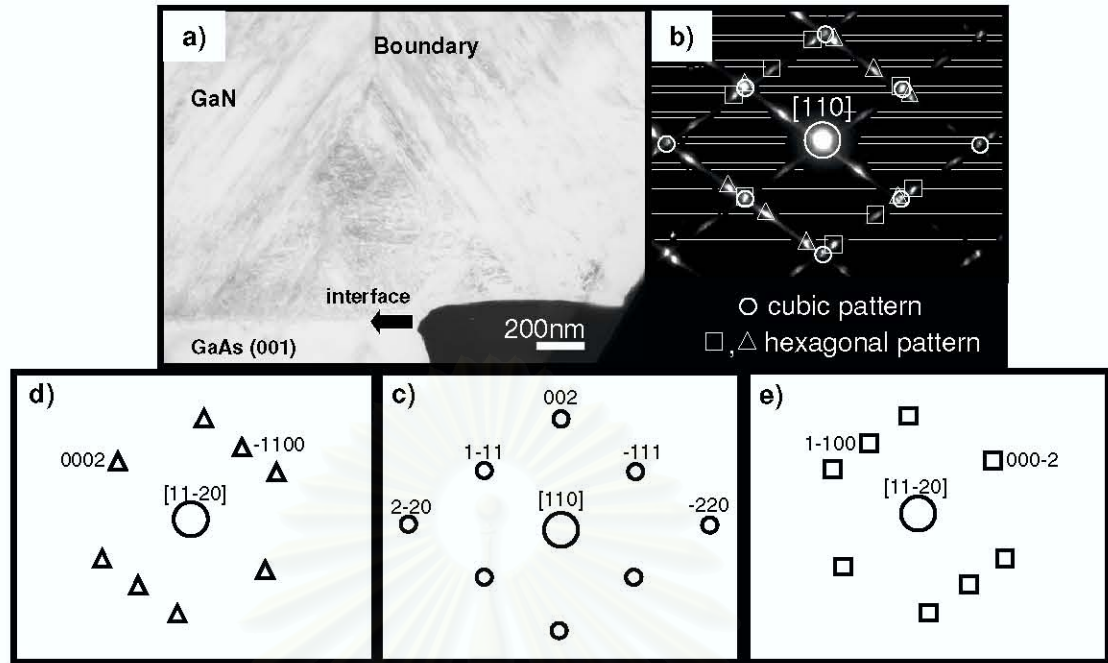


Figure 4.5: a) Microstructure of the GaN region containing the pyramid-like structure for the GaN layer grown at 960°C. b) Selected area diffraction (SAD) records along $\langle 110 \rangle$ *c*-GaN from the GaN region containing the pyramid-like structure. Schematic representation of Fig. 4.5 b) showing c) and e) hexagonal and d) cubic phase diffraction spots. Diffraction patterns obtained from the grain boundary regions, showing 70.5° rotation of *h*-GaN crystal around $\langle 11-20 \rangle$.

GaAs (001) substrates at the growth temperatures of 900°C (Figs. 4.4 a) and b)) and 960°C (Figs. 4.4 c) and d)). For the lower growth temperature (900°C), the SAD pattern from the interface portion clearly indicates that the GaN grown layer has the cubic structure (Fig. 4.4 b)). No different type of single diffraction spots on the SAD pattern was observed. However, the microstructure is characterized by a high density of stacking faults close to the interface (Fig. 4.4 a)), which results in streaking of diffraction spots on the SAD pattern (Fig. 4.4 b)). Besides, the streaks with small intensity maxima at the position marked by arrows indicate that the regions with SFs tend to have a hexagonal stacking sequence. On the other hand, for the higher growth temperature (960°C), the SAD pattern (Fig. 4.4 d)) shows a different type of single diffraction spots, indicating the incorporation of single-crystal *h*-GaN in the 960°C grown layer. A high density of pyramid-like structures

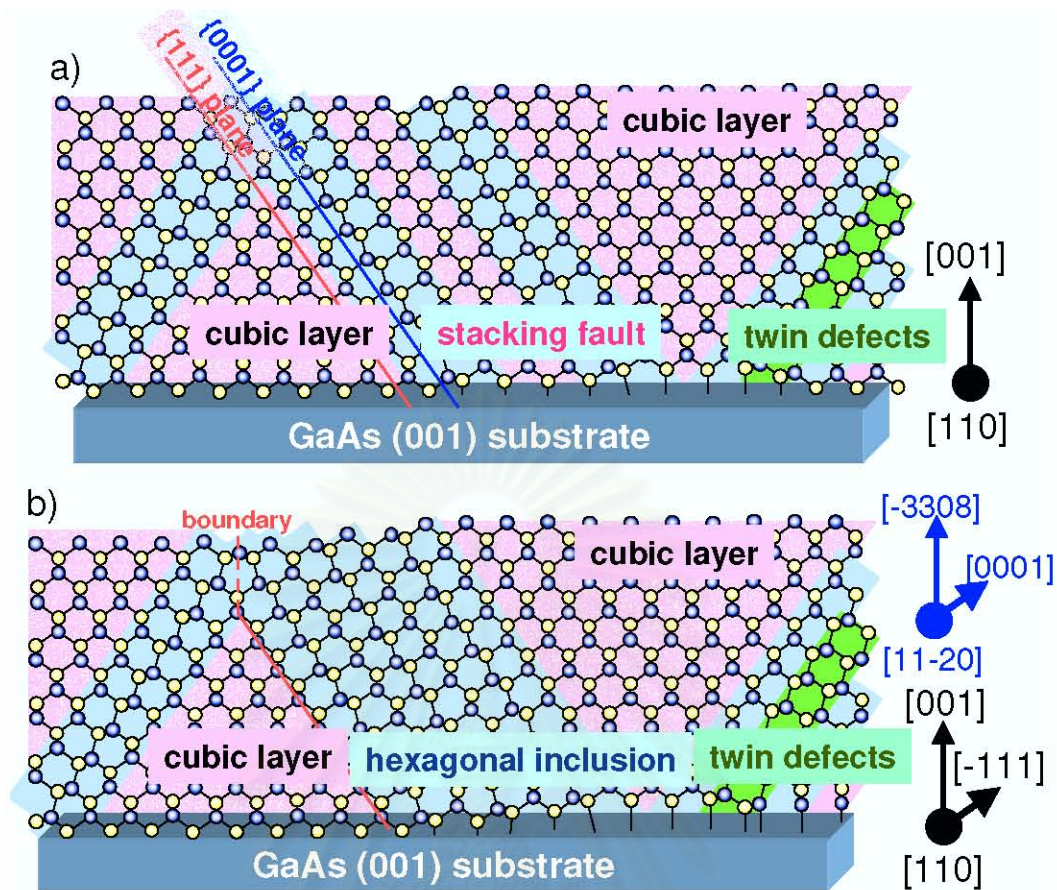


Figure 4.6: Schematic illustrations of the (110) cross-section view of main crystal-defects generated in the *c*-GaN films grown on GaAs (001) substrates at growth temperatures a) 900°C and b) 960°C

showing (1-11) and (111) facets and looking like penetrating into the GaN layers are clearly observed at the interface (Fig. 4.4 c)). It is known that the occurrence of a hexagonal-like stacking mode is naturally expected since GaN is usually stable in hexagonal structure. These results suggest that SFs, if densely accommodated, can become seeds of *h*-GaN structure in the layer of *c*-GaN [32]. Figure 4.5 shows another cross-sectional TEM image of the region containing the pyramid-like structure for the 960°C grown *c*-GaN layer. The SAD pattern obtained from the same region, as shown in Fig. 4.4 b), illustrates the observed orientation relationship between the *h*-GaN and the *c*-GaN. This indicates that the orientation relationship between the *c*-GaN and hexagonal inclusions is $\{111\} // \{0002\}$ and $\langle 110 \rangle // \langle 11-20 \rangle$. Figure 4.6 b) shows the schematic illustration of the hexagonal

inclusions in the *c*-GaN at high growth temperature, comparing with that of the stacking faults in the *c*-GaN at 900°C, as shown in Fig. 4.6 a). It also appears that the *h*-GaN seeds in the pyramid-like structure area rotated by 70.5° to each other around the $\langle 11\bar{2}0 \rangle$ axis (Figs. 4.5 c) - 4.5 e)). The boundary plane was parallel to $\{3\bar{3}08\}$ plane of both sides of the *h*-GaN crystal seeds (Fig. 4.5 a)), showing a symmetric tilt boundary. In addition, the boundary is shown as a red line in Fig. 4.6.

The observations described above demonstrate that the growth temperature much affect the selection of the growth of cubic and hexagonal structures. It is plausible that the cubic-to-hexagonal polytype transition can be controlled by an appropriate growth temperature as well as by crystal symmetry of substrate surfaces. In fact, we found that the *c*-GaN layers grown on GaAs (001) substrates at the growth temperature about 900°C prior to the growth of GaN, *c*-GaN without mixing with a single crystal hexagonal phase can be obtained [15, 32].

4.3 Summary

The effect of growth temperature on the polytype translation of GaN grown on GaAs (001) substrates by MOVPE were been investigated. It was found by XRD measurements and TEM observations that the GaN grown layers exhibited a transition from cubic to mixed cubic/hexagonal phase under conditions of increasing the growth temperature from 900 to 960°C. The GaN films with the cubic phase purity higher than 85 percent were achieved for the low growth temperature of 900°C [30]. For such high cubic phase purity GaN layers, no different types of single diffraction spots, indicating the incorporation of single-crystal *h*-GaN, on the SAD pattern was observed. In addition, the PL from these GaN layers confirms the existence of transition from cubic to hexagonal phases in microstructure of the GaN grown layers as the growth temperature increased. We suggest that the growth temperature is a key parameter in the growth of high cubic phase purity *c*-GaN films without incorporation of single-crystal *h*-GaN.

CHAPTER V

STRUCTURAL PHASE TRANSITIONS IN SAG-*c*-GaN FILMS

In this chapter, the selective-area grown cubic GaN (SAG-*c*-GaN) film was selected to investigate correlation between the generation of *h*-GaN and the growth features of SAG *c*-GaN film. In this study, the SAG-*c*-GaN film, *h*-GaN was fabricated along (111) *c*-GaN surfaces. The film composed of (311) and (111) facets as the top surface and the sidewalls, respectively, was characterized by scanning electron microscopy (SEM) and transmission electron microscopy (TEM). It was found that the single crystal *h*-GaN was laterally overgrown on the (111) *c*-GaN surfaces during the growth, indicating that *h*-GaN is easily constructed along (111) facets. In addition, the characteristics of the single-crystal GaN regions, obtained by selective-area and subsequent lateral overgrowth on the stripe-patterned GaAs (001) substrates by MOVPE, is described.

5.1 Overview of SAG-*c*-GaN

A selective-area growth (SAG) is the method of epitaxial growth on partially masked substrates. There are many experimental data proving that the SAG reduces dislocation density by blocking the dislocation propagation from the substrate using oxide masks [33, 34]. The parts of SAG layers grown laterally are nearly defect-free in spite of a high density of dislocation in the layer grown

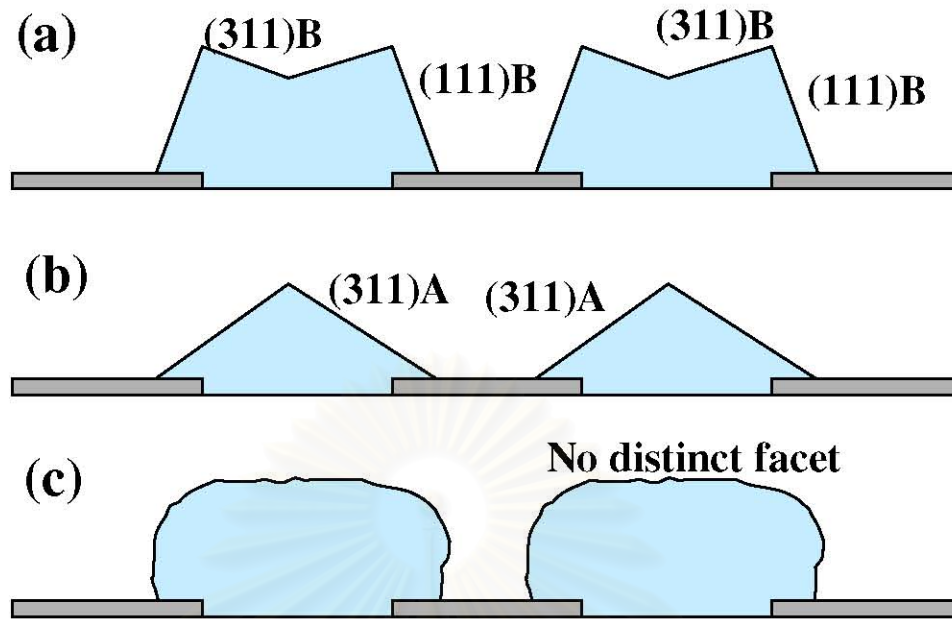


Figure 5.1: A schematic of three types of growth feature for SAG *c*-GaN grown using stripe opening along a) [110], b) [1-10] and c) [100] directions, respectively [33]

directly on substrate. Therefore, the SAG is the promising method to produce GaN films with a low density of extended crystal defects. Recently, Sanorpim et al.[36] have reported that the *c*-GaN structures using SAG can be controlled by mask direction and mask fill factor. Figure 5.1 shows the three possible types of growth features for the SAG *c*-GaN stripes on different mask stripe orientations. They also reported that a major problem in SAG *c*-GaN is to provide high cubic phase purity without incorporation of *h*-GaN. Since it is well known that the single crystal *h*-GaN is easily generated along the (111) facets [35]. Then, we select the SAG-*c*-GaN film which is composed of (111) facets as the sidewalls to study the correlation between the crystal structure and the growth feature of the film.

The SAG-*c*-GaN film used in this study was grown using MOVPE [36]. TMG, DMHy and AsH₃ were used as Ga, N and As precursors, respectively. H₂ was used as carrier gas. A 200-nm-thick SiO₂ mask pattern with [110]-stripe orientation on GaAs (100) substrate designed by photolithography was used. The ratio of the open width to the pattern period (fill factor) of 0.5 was used. The

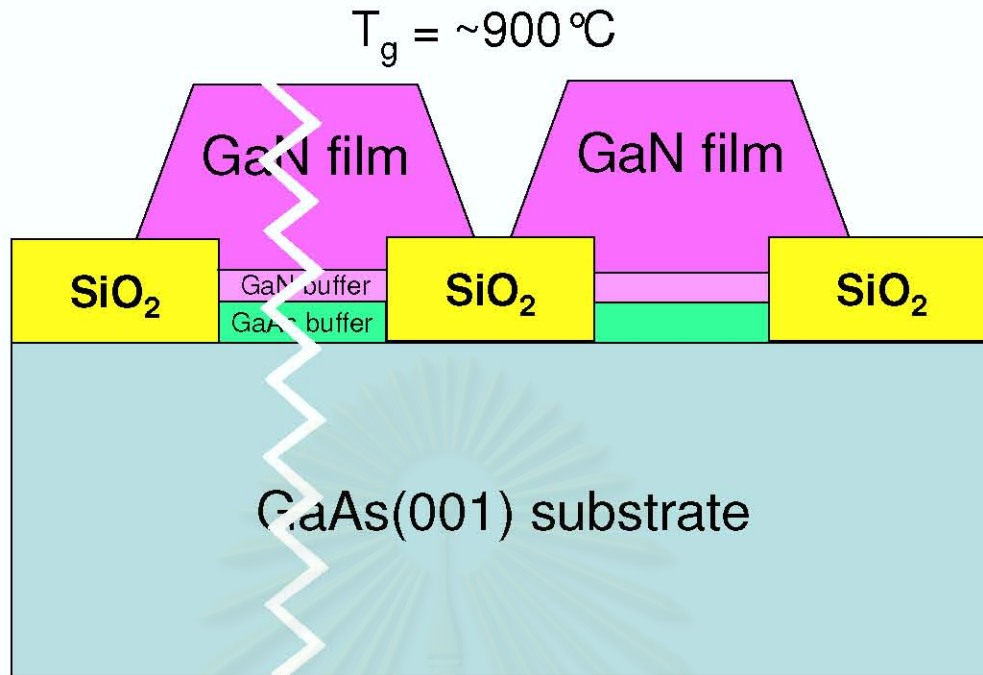


Figure 5.2: Schematic illustration of SAG *c*-GaN films on stripe patterned GaAs (001) substrate along the [110] orientation at growth temperature of 900°C. W and M indicate the window and SiO₂ mask regions, respectively.

c-GaN film was grown on these patterned substrates. After the deposition of ~ 100 -nm-thick GaAs buffer layer at 700°C, the 20-nm-thick low temperature (LT)-grown GaN buffer layer was grown at 600°C. Finally, the *c*-GaN epitaxial layer was deposited for 15 min. The growth temperature and V/III ratio were maintained at 900°C and 25, respectively. Thickness of the grown *c*-GaN layers was examined to be 2-3 μm . Figure 5.2 show an illustration of SAG *c*-GaN films on stripe patterned GaAs (001) substrate along the [110] orientation. W and M indicate the window and SiO₂ mask regions, respectively.

5.2 Growth feature of SAG *c*-GaN

The GaN layer was not like a sheet, as shown in Chapter 3 and 4, but like a stripe pillar lying along a mask stripe in morphology. Figure 5.3 shows the surface and cross-sectional morphology of the GaN layer grown on stripe patterned GaAs

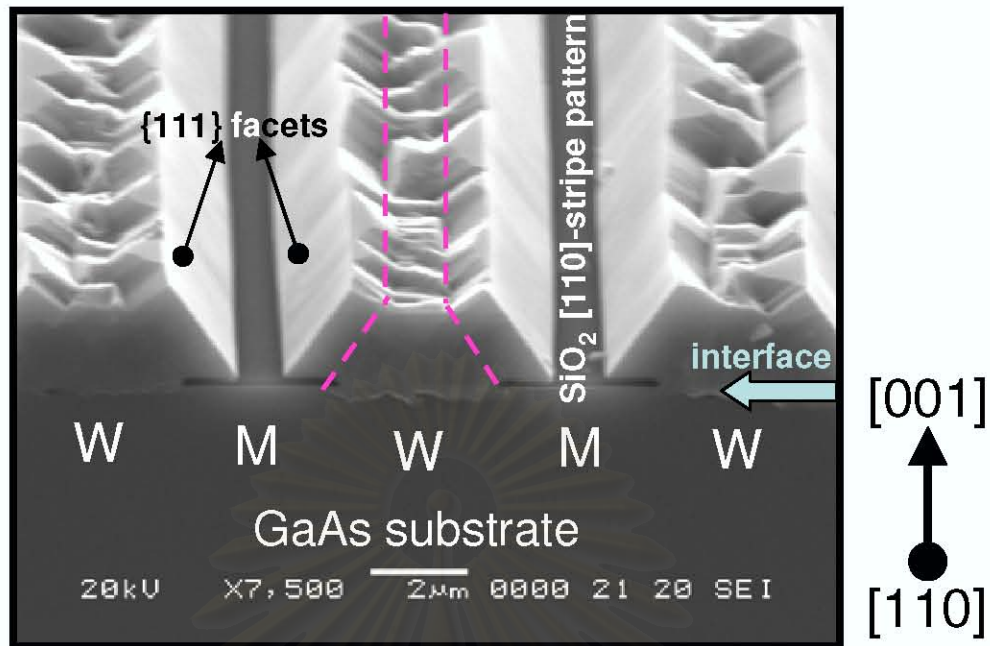


Figure 5.3: Cross-sectional SEM micrograph of SAG-*c*-GaN on stripe patterned GaAs (001) substrate at growth temperature of $\sim 900^\circ\text{C}$.

(001) substrate along the [110] direction. A trapezoidal shape with inclined (311) top surface and flat sidewall (111) facets was clearly seen. Such facet planes were very reproducible at this growth condition and were also observed for the samples with different growth times of 30 and 90 min and different growth temperatures [2]. Thus, these results indicated that the (111) facets are quite stable during the growth. In addition, the growth of GaN only occurs within the window regions, indicating the excellent selectivity of GaN growth with the SiO_2 amorphous mask. Distinguish contrasts between lateral region and on the window region was found as indicated by dashed lines. It is interesting that how the *h*-GaN is generated in the SAG-*c*-GaN film which is composed of the sidewalls with (111) facets?

5.3 TEM investigation of SAG *c*-GaN

As shown in Fig. 5.4, low-resolution cross-sectional TEM micrograph shows the surface and cross-sectional morphologies of the GaN stripe along the [110]

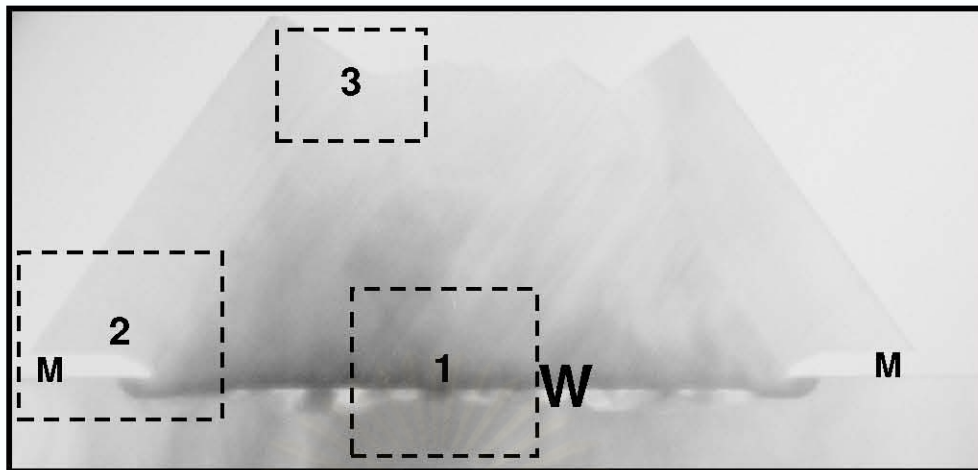


Figure 5.4: Cross-sectional TEM micrograph in the $[110]$ -oriented stripe pattern showing laterally overgrown GaN layer on SiO_2 mask.

direction. It is clearly seen that the feature of the GaN stripe is a trapezoidal shape with rough surface and very flat sidewall (111) facets. Note that the contrast between GaN regions above the SiO_2 mask and on the window is clearly observed. This contrast may be attributed to the difference in crystal structure between these two regions.

Figure 5.5 a) shows a higher resolution cross-sectional TEM micrograph taken from the GaN on the window area, **Region 1** in Fig.5.4. Two distinctive regions of GaN and GaAs substrate are clearly seen. The stacking faults density drastically decreasing away from the substrate toward the top surface of *c*-GaN stripe was also observed. The result of ED pattern from this corresponding region demonstrates (Fig. 5.5) that GaN grown within the window area shows the same crystal structure (cubic phase) as that of GaAs substrate. Furthermore, there is an evidence that the (111) faulting is associated with roughening and the local strain at the interface.

The microstructure of the laterally overgrown GaN region above the SiO_2 mask, **Region 2** in Fig. 5.4, for the stripe window oriented along the $[110]$ direction is shown in Fig. 5.6. It was observed that the GaN region on the SiO_2 mask is nearly defect free *h*-GaN with low density of short dislocation segments.

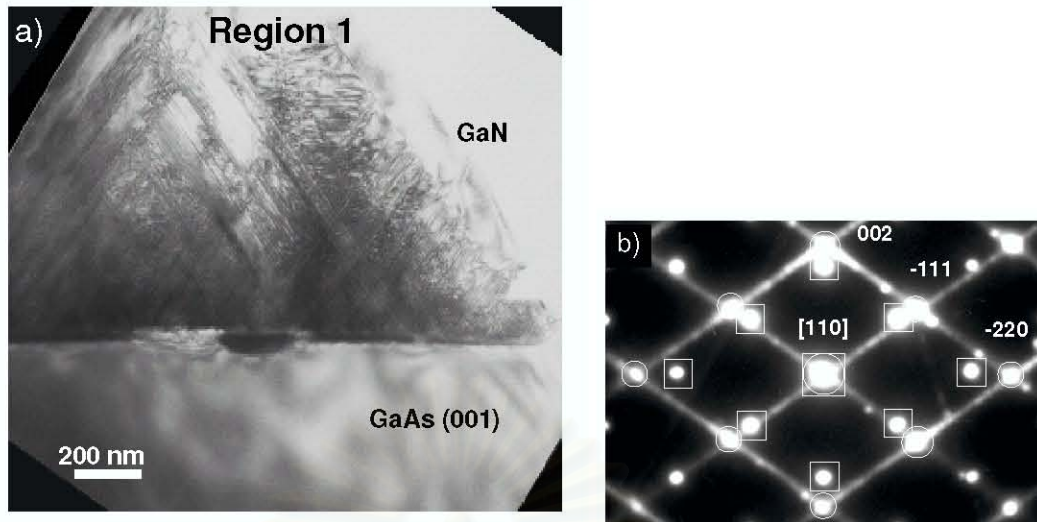


Figure 5.5: a) Cross-sectional TEM micrograph of GaN on the window (**Region 1** in Fig. 5.4) b) Corresponding electron diffraction (ED) patterns taken near the $[110]$ zone axis.

No stacking faults and twins in the laterally overgrown regions were observed. The dislocation density in the laterally overgrown h -GaN regions was estimated to be lower than 10^8 cm^{-2} which is two orders of magnitude smaller than the dislocation density in conventionally grown h -GaN films. Although additional microstructural studies are required to fully understand dislocation evolution during SAG, Fig. 5.6 a) clearly indicates that the dislocations, generating from the h -GaN/ c -GaN interface, propagate to the (0001) surface of the laterally overgrown h -GaN.

Figure 5.7 shows cross-sectional TEM micrograph and the ED pattern of top surface region, **Region 3** in Fig. 5.4. The ED pattern demonstrates orientation relationship between the h -GaN and the c -GaN regions in the SAG c -GaN stripes along the $[110]$ direction. The inference of this observation are $(1-11)_{c\text{-GaN}} // (000-2)_{h\text{-GaN}}$ and $[110]_{c\text{-GaN}} // [11-20]_{h\text{-GaN}}$, which are the same as the investigated results of c -GaN film described in the section 4.2. These results demonstrate that although the c -GaN film is grown at the low growth temperature ($\sim 900^\circ\text{C}$), the h -GaN still be constructed along the (111) facets. A schematic illustration of the generation of h -GaN on $(111)_{c\text{-GaN}}$ is shown in Fig. 5.8. In fact, the lattice mismatch between $(0002)_{h\text{-GaN}}$ and $(111)_{c\text{-GaN}}$ is less than 0.01 percent, resulting

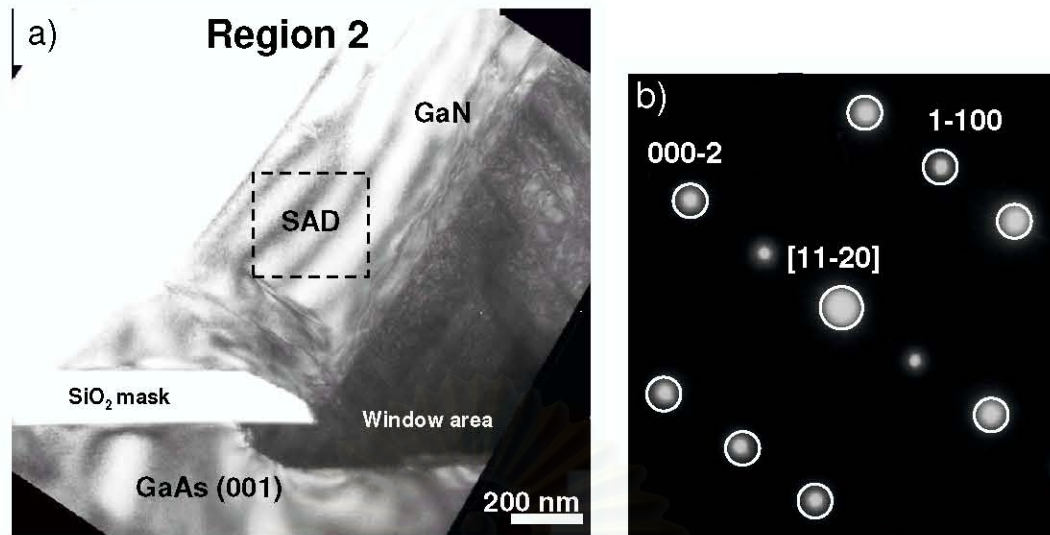


Figure 5.6: a) Cross-sectional TEM micrograph of GaN on the SiO₂ mask (**Region 2** in Fig. 5.4) b) Corresponding electron diffraction (ED) patterns taken near the [110] zone axis.

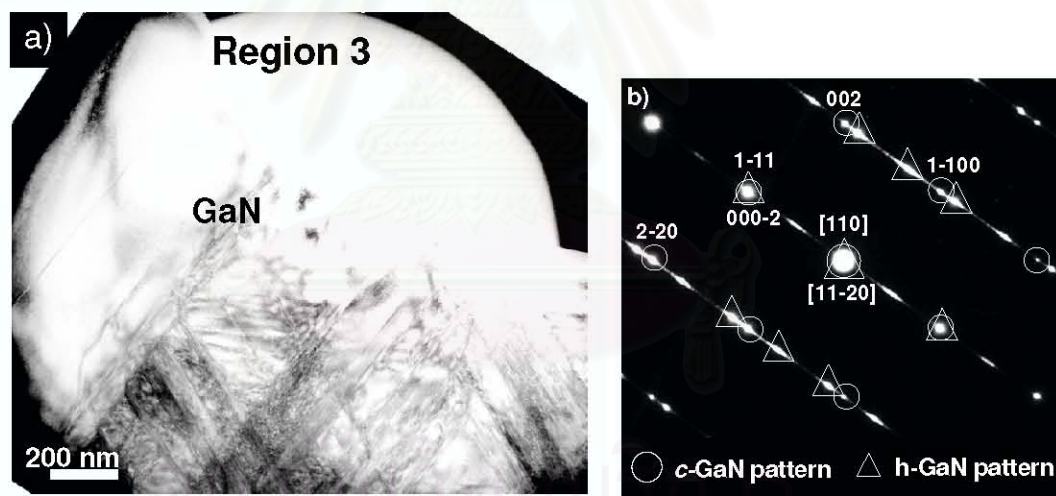


Figure 5.7: a) Cross-sectional TEM micrographs of top surface region (**Region 3** in Fig. 5.4) b) Corresponding selected area diffraction (SAD) patterns taken near the [110] zone axis.

in a large reduction of the dislocation density near the (0001) surface regions. It is suggested that the lateral overgrown *h*-GaN is also obtained using the stripe patterned GaAs (001) substrate as well as the non-patterned sapphire (0001), SiC (0001) and GaAs (111) substrates.

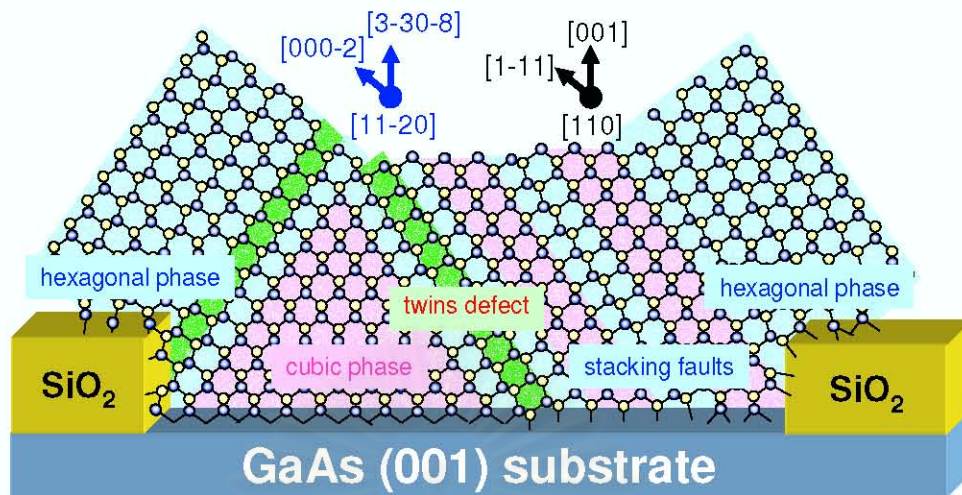


Figure 5.8: (Schematic illustration of the (110) cross-sectional SAG *c*-GaN layer grown on the stripe patterned GaAs (001) substrate at the growth temperature of 900°C.

5.4 Summary

The correlation between the crystal structure and the growth feature of the SAG-*c*-GaN film grown at growth temperature of 900°C was investigated. The trapezoid shape of the GaN stripes bounded with (311) top and (111) sidewalls was clearly observed by SEM and low resolution TEM. Based on TEM measurements, the GaN region on window is still *c*-GaN, while the nearly free *h*-GaN was observed on the SiO₂ mask. In addition, we found that the $(1-11)_{c-GaN} // (000-2)_{h-GaN}$ and $[110]_{c-GaN} // [11-20]_{h-GaN}$ were found at low growth temperature. These results confirmed that *h*-GaN is considerably constructed along the (111) facets of *c*-GaN even though at the low growth temperature (900°C).

CHAPTER VI

CONCLUSIONS

In this thesis, the author was described a detailed study of the structural properties of the *c*-GaN films grown on GaAs (001) substrates by MOVPE. The transmission electron microscopy (TEM) analysis was mainly used to investigate the main structural defects in the GaN films. The discussion was focused on the *c*-GaN films with high cubic phase purity, where several experimental works have been done. As a result, fundamental understanding of the defect generation in the *c*-GaN films were obtained. The main results and conclusions obtained in this study are summarized as follows:

(1) The preparation of the *c*-GaN/GaAs samples for TEM investigation was studied and described. The large different hardness between two regions of the sample, namely the *c*-GaN layer and the GaAs substrate, was carefully taken to obtain the sample thickness in micro-scale with the smooth morphology. The prepared samples had essential conditions for TEM investigation.

(2) The structural defect in the *c*-GaN film grown at low growth temperatures of 900-920°C was mainly analyzed from electron diffraction (ED) patterns and cross-sectional micrograph of TEM measurements. The results demonstrate that the GaN grown film has a cubic structure, which is confirmed by the ratio of the integrated ω -scan XRD intensities of the cubic (002) and hexagonal (1-101) planes. It is also confirmed that the cubic phase purity higher than 85 percent was achieved. On the other hand, a high density of planar defects such as stacking faults and twins on the 111 cubic plane were clearly observed. This result suggests that the main defects in such high cubic-phase-purity GaN films are the stacking faults and twins. It is important to note that no indication of *h*-GaN single crystal

was observed in this *c*-GaN film.

(3) The polytype transition of GaN grown on GaAs (001) substrates by MOVPE were investigated. It was found by XRD measurements and TEM observations that the GaN grown layers exhibited a transition from cubic to mixed cubic/hexagonal phase under the condition of increasing the growth temperature from 900 to 960°C. The GaN films with the cubic phase purity higher than 85 percent were achieved for the low growth temperature of 900°C. For such high cubic phase purity GaN layers, no different types of single diffraction spots, indicating the incorporation of single-crystal *h*-GaN, on the SAD pattern was observed. In addition, the PL from these GaN layers confirms the existence of transition in microstructure of the GaN grown layers as the growth temperature increased. It is suggested that the growth temperature is a key parameter in the growth of high cubic phase purity *c*-GaN films without incorporation of single-crystal *h*-GaN. Our results demonstrate that the main defects in *c*-GaN films grown at high growth temperature (960°C) are SFs, twins and hexagonal phase inclusion.

(4) To investigate structural phase transition from cubic to hexagonal structures, the SAG *c*-GaN film with (111) surface morphologies grown on the stripe-patterned GaAs (001) substrate at low growth temperature of 900-920°C was studied by TEM. The SAD patterns illustrated the $(1-11)_{c-GaN} // (000-2)_{h-GaN}$ and $[110]_{c-GaN} // [11-20]_{h-GaN}$. It is confirmed that *h*-GaN considerably constructed along the (111) facets of *c*-GaN even at low growth temperature (900°C). The result in this part clearly demonstrate that the formation of (111) facets during the growth is more important parameter for the growth of the *c*-GaN films with high cubic-phase-purity than the growth temperature.

As shown by these results, the structural defects in the *c*-GaN films grown on GaAs (001) substrate are stacking fault and twin as well as hexagonal inclusion. It is found that the growth temperatures and the grown surface morphologies are mainly affecting parameters on the hexagonal phase generation in the *c*-GaN film. To grow high quality *c*-GaN film without incorporation of hexagonal inclusion, the appearance of {111} facets on the grown surface should be eliminated during the growth. The growth should be also performed at an appropriate growth tem-

perature (900-920°C). The results obtained here can be used not only to interpret the *c*-GaN films; but may also be extended to explain the structural properties of other III-Nitride semiconductors. Hopefully, the obtained information is very useful for the full understanding of mechanism of defect generation in the III-Nitride based devices. Further work is still necessary to fully clarify the affecting parameters on the hexagonal phase generation in the thin film growth of III-Nitride semiconductors.



สถาบันวิทยบริการ
จุฬาลงกรณ์มหาวิทยาลัย

REFERENCES

- [1] Yu Jen Hsu, Lu Sheng Hong, Jyh Chiang Jiang, and Jing Chong Chang, Effects of hydrogen on GaN metalorganic vapor-phase epitaxy using tertiarybutylhydrazine as nitrogen source, *J. Crystal Growth* **266** (2004): 347-353.
- [2] J. Wu, M. Kudo, A. Nagayama, H. Yaguchi, K. Onabe, and Y. Shiraki, Selective Growth of Cubic GaN on Patterned GaAs (100) Substrates by Metalorganic Vapor Phase Epitaxy, *phys. stat. sol.* **176** (1999): 558.
- [3] H. Chen, Z.Q. Li, H.F. Liu, L. Wan, M.H. Zhang, Q. Huang, J.M. Zhou, Y. Luo, Y.J. Han, K. Tao, and N. Yang, Controllable cubic and hexagonal GaN growth on GaAs(001) substrates by molecular beam epitaxy, *J. Crystal Growth* **210** (2000): 811.
- [4] S. Marlafecka, N. Bock, T.S. Cheng, S.V. Novikov, A.J. Winsor, I. Harrison, C.T. Foxon, and P.D. Brown, A structural study of phase transitions within GaN layers grown by low-temperature molecular beam epitaxy, *J. Crystal Growth* **230** (2001): 415.
- [5] In Hyung Lee, and Seung Min Park, Deposition of Cubic GaN Films by Reactive Laser Ablation of Liquid Ga Target in Ammonia, *Bull. Korean Chem. Soc.* **21/11** (2000): 1065.
- [6] Chin-Yu Yeh, Z.W.Lu, S. Froyen, and Alex Zunger, Zinc-blende-wurtzite polytypism in semiconductors, *Phys. Rev. Lett.*, **24/25** (1992): 10094.
- [7] S. Fujieda, and Y. Matsumoto, Structure Control of GaN Films Grown on (001) GaAs Substrates by GaAs Surface Pretreatments, *Jpn. J. Appl. Phys.* **30** (1991): L1665.
- [8] M. Sato, Plasma-Assisted Low-Pressure Metalorganic Chemical-Vapor-Deposition of GaN on GaAs Substrates, *J. Appl. Phys.* **78** (1995): 2123.

- [9] T. Lei, T.D. Moustakas, R.J. Graham, Y. He, and S.J. Berkowitz, Analysis of Unstable Two-Phase Region in Wurtzite Group III Nitride Ternary Alloy Using Modified Valence Force Field Model, *J. Appl. Phys.* **71** (1992): 4933.
- [10] H. Okumura, S. Yoshida, and T. Okahisa, Optical properties near the band gap on hexagonal and cubic GaN, *Appl. Phys. Lett.* **64** (1994): 2997.
- [11] R. C. Powell, N.-E. Lee, Y.-W. Kim, and J.E. Greene, Heteroepitaxial wurtzite and zinc-blende structure GaN grown by reactive-ion molecular-beam epitaxy: Growth kinetics, microstructure, and properties, *J. Appl. Phys.* **73** (1993): 189.
- [12] H.F.Liu, H. Chen, L. Wan, Z.Q. Li, Q. Huang, and J.M.Zhou, Epitaxial growth and characterization of GaN Films on (001) GaAs substrates by radio-frequency molecular beam epitaxy, *J. Crystal Growth* **227-228** (2001): 390-394.
- [13] S. Sanorpim, E. Takuma, K. Onabe, H. Ichinose, and Y. Shiraki, Laterally Overgrown GaN on Patterned GaAs (001) Substrates by MOVPE, *phys. stat. sol., (a)* **192** (2002) : 446.
- [14] Yeonjoon Park, Michael J. Cich, Rian Zhao, Petra Specht, and Eicke R. Weber, Analysis of twin defects in GaAs (111)B molecular beam epitaxy growth, *J. Vac. Sci Technol.* **18** (2000): 1566-1571.
- [15] S. Sanorpim, J. Wu, K. Onabe, and Y. Shiraki, Effects of growth temperature in selective-area growth of cubic GaN on GaAs (100) by MOVPE, *J. Crystal Growth* **237-239** (2002): 1124-1128.
- [16] X.M. Shen, Y.T. Wang, X.H. Zheng, B.S. Zhang, J. Chen, G. Feng, and H. Yang, X-ray diffraction analysis of MOCVD grown GaN buffer layers on GaAs (001) substrates, *Journal of Crystal Growth*, **254** (2003) : 23.
- [17] Y. Ge Yang, H. Lei ma, C. Shan Xue, X. Tao Hao, H. Zhao Zhuang, and J. Ma, Characterization of GaN films grown on silicon (111) substrates, *Physica B*, **325** (2003) : 230.

- [18] S. Sanorpim, J. Wu, K. Onabe, and Y. Shiraki, Detection and Analysis of Hexagonal Phase Generation in Selective-Area Growth of Cubic GaN by Metalorganic Vapor Phase Epitaxy, *IPAP Conference Series*, **Series 1** (2000) : 89-92.
- [19] X.M. Shen, G. Feng, B.S. Zhang, L.H. Duan, Y.T. Wang and H. Yang, Selective area growth of GaN on GaAs (001) substrates by metalorganic vapor-phase epitaxy, *Journal of Crystal Growth*, **252** (2003) : 9.
- [20] E. Kim, I. Rusakova, I. Berishev, A. Tempez, and A. Bensaoula, GaN thin film growth on GaAs (001) by CBE and plasma-assisted MBE, *Journal of Crystal Growth*, **243** (2002) : 456.
- [21] C. Chia-Hao, *Electronic structure investigations of group III-nitrides surface and interfaces*. Master's thesis, School of Mathematics and Natural Sciences, Technical University of Berlin, **Germany**, 2003.
- [22] H.Tsuchiya, K. Sunaba, S. Yonemura, T. Suemasu, and F. Hasegawa, Cubic Dominant GaN Growth on (001) GaAs Substrates by Hydride Vapor Phase Epitaxy, *J. Crystal Growth* **189/190** (1998): 231-243.
- [23] David B. Williams, and C. Barry Carter, *Transmission Electron Microscopy: A Textbook for Materials Science*. New York: A Division of Plenum Publishing Corporation, 1996.
- [24] M.H. Loretto *Electron Beam Analysis of Materials*. 2nd ed. London: Chapman-Hall, 1994.
- [25] B.D.Cullity, *Elements of X-ray diffraction*. 2nd ed. Massachusetts: Addison Wesley, 1978.
- [26] H. Okumura, K. Ohta, G. Feuillet, K. Balakrishnan, S. Chichibu, H. Hamaguchi, P. Hacke, and S. Yoshida, Growth and characterization of cubic GaN, *J. Crystal Growth*, **178** (1997) : 113-133.
- [27] H. P. Maruska, and J. J. Tiejen, The preparation and properties of. vapor-deposited single-crystalline GaN, *Appl. Phys. Lett.*, **15** (1969) : 327.

- [28] B. Fultz, and J. Howe, *Transmission Electron Microscopy and Diffractometry of Materials*. 2nd ed. Tokyo: Springer, 2002.
- [29] J. Wu, H. Yaguchi, H. Nagasawa, Y. Yamaguchi, K. Onabe, Y. Shiraki, and R. Ito, Crystal Structure of GaN Grown on 3C-SiC Substrates by Metalorganic Vapor Phase Epitaxy, *Jpn. J. Appl. Phys.* **36** (1997): 4241.
- [30] I. Akasaki, H. Amano, S. Sota, H. Sakai, T. Tanaka, and M. Koike, Stimulated Emission by Current Injection from an AlGaIn/GaN/GaInN Quantum Well Device, *Jpn. J. Appl. Phys.* **34** (1995): L1517.
- [31] K. Onabe, J. Wu, R. Katayama, F. H. Zhao, A. Nagayama and Y. Shiraki, Cubic GaN Films on GaAs (001) Substrates without Deep-Level Luminescence Grown by Metalorganic Vapor Phase Epitaxy, *phys. stat. sol.(a)* **180** (2000): 15-19.
- [32] N. Kuwano, Y. Nagatomo, K. Kobayashi, K. Oki, S. Miyoshi, H. Yaguchi, K. Onabe, and Y. Shiraki, Transmission Electron Microscope Observation of Cubic GaN Grown by Metalorganic Vapor Phase Epitaxy with Dimethylhydrazine on (001) GaAs, *Jpn. J. Appl. Phys.* **33** (1994): 18.
- [33] T. S. Zheleva, O. H. Nam, M. D. Bremser, and R. F. Davis, Dislocation density reduction via lateral epitaxy in selectively grown GaN structures, *Appl. Phys. Lett.* **71** (1997): L2638.
- [34] A. Usui, H. Sunakawa, A. Sakai, and A. Yamaguchi, Thick GaN Epitaxial Growth with Low Dislocation Density by Hydride Vapor Phase Epitaxy, *Jpn. J. Appl. Phys.* **36** (1997): L899.
- [35] J. Wu, M. Kudo, A. Nagayama, H. Yaguchi, K. Onabe, and Y. Shiraki, Homoepitaxial Growth and Luminescence Characterization of GaN Epilayer by RF-MBE on MOCVD-Grown GaN Substrate, *phys. Stat. Sol. (a)* **176** (1999): 463.
- [36] S. Sanorpim, J. Wu, K. Onabe, and Y. Shiraki, *Proc. Int. Workshop on Nitride Semiconductors, IPAP Conf. Series 1* (2000): pp.89-92.

VITAE

Miss Siripen Suandon was born on November 11, 1979 in Phichit, Thailand. She received her Bachelor degree of Science in Physics from Chulalongkorn University in 2000, and continued her Master's study in 2003.

Publications and Conference Presentations:

[1] **S. Suandon**, S. Sanorpim, K. Yoodee and K. Onabe, 'Investigation of stacking fault and twin defects in MOVPE grown cubic GaN on GaAs', (2005) Journal of Scientific Research, Chulalongkorn University, Section T (J. Sci. Res. Chula. Univ. Section T), 3 (3), 291-300.

[2] **S. Suandon**, S. Sanorpim, K. Yoodee and K. Onabe, 'Effect of growth temperature on polytype transition of GaN from zincblende to wurtzite', (2006) Thin Solid films, accepted.

1. **Siripen Suandon**, Sakuntam Sanorpim, Kajornyod Yoodee and Kentaro Onabe 'Effect of Growth temperature on Polytype transition of GaN from zincblende to wurtzite' *The 3rd International Conference on Materials for Advanced Technologies (ICMAT 2005)*, The Materials Research Society of Singapore, Singapore, July 3-8, 2005.

2. **Siripen Suandon**, Sakuntam Sanorpim, Kajornyod Yoodee and Kentaro Onabe. 'TEM Investigation of Polytype Transition of GaN from Cubic to Hexagonal' *13th Academic Conference*, Faculty of science, Chulalongkorn University, Thailand, March 16-17, 2005.

3. **Siripen Suandon**, Sakuntam Sanorpim, Kajornyod Yoodee and Kentaro Onabe. 'A structural study of phase transitions within selected area growth of cubic GaN by MOVPE' *The 5th National Symposium on Graduate Research*, The Graduate School, Kasetsart University, Thailand, October 10-11, 2005.

4. **Siripen Suandon**, Sakuntam Sanorpim, Kajornyod Yoodee and Kentaro Onabe. 'Investigation of hexagonal phase generation in cubic GaN films on GaAs' *30th Congress on Science and Technology of Thailand (STT 2005)*, Suranaree University of Technology, Thailand, October 18-20, 2005.